# Responses to Anonymous Referee #1

Interactive comments on:

**Optimizing UV index determination from broadband irradiances**
**by**
**Keith A. Tereszchuk et al.**

Provided by: Anonymous Referee #1
Received and published: 31 December 2017

Preamble: In addition to the changes made to the manuscript following the suggestions of the two reviewers, we also identified three minor issues that required performing a re-analysis of the data and also modifying comments regarding the comparison to Brewer measurements of Section 2.2. These changes did result in a small correction in the scaling and fit factors, but results remain essentially the same (other than improving the agreement with Brewer UV irradiances). These points are as follows:

1. An adjustment of the broadband wavelength boundaries from 280, 294, 310, and 400 nm to 280.11, 294.12, 310.70, and 400.00 nm (this was an error)

2. A correction in applying a moving boxcar averaging window covering $\pm 0.25$ nm about sampling points at intervals of 0.5 nm

3. A correction in the calculation of differences with the Brewer UV spectra in Section 2.2, resulting, most significantly, in a reduction of the mean percent differences for the 311-330 nm band from 7.5% to 2.9% (and implying related text changes).

The correction of few other typographical errors were also made.

The following are general comments and questions:

I am not accustomed to seeing correlations expressed as percent, rather as a unitless values ranging from -1.0 to 1.0.

The root mean square relative error calculation provides a more tangible, quantitative, overall representation of the errors and their scatter. Percentages were used to determine the absolute range of values that were encountered. While the Pearson correlation coefficient, R (ranging from -1.0 to 1.0), which provides a value which represents the "goodness" of the fit in a linear correlation, could also have been calculated and shown, the root mean square errors (and mean differences) were considered sufficient and more appropriate for our purpose, in addition to presenting the scatter plot themselves.

This is a rhetorical question: Which is preferred : 'UV index' or 'UV Index'? Even the WMO web page has a mixture of both. But its acronym is 'UVI' implying that 'index' is capitalized.

While, we are not aware of a definitive preference, one could choose to follow the convention of a capitalized 'index' considering the often used acronym 'UVI'. The format for using the lower case i in this work was simply done to avoid any possible conflicts with the manuscript composition guidelines with regard to figures, section titles, etc that have been detailed by the publisher, while trying to maintain consistancy throughout the paper. Having said that, we see now that there are 2-3 times where consistancy was not maintained. The manuscript has therefore been edited so that 'UV Index' appears using only the uppercase I and the term is treated as a proper name where the word index should be capitalized.

Comments, questions:
P2, L20: Should be 'oxygen (O2)'.

Correction made.

P2, L27: Expand on what is meant by 'more sensitive population.

Changed to more photosensitive populations. This refers to people who have extremely little melanin/skin pigmentation which provides a natural UV barrier. There are also a number of ailments where minimal doses of UV radiation can cause allergic reactions and severe burns. Increased photosensitivity can also present itself as a side effect for a variety of medications.

P3, L4: 'erythemal action spectrum (EAS)'

Correction made.

P3, L15 The UVI does not have to be an integer.

The word 'integer' has been removed.

P3, L17 The tropics have high UVI values not just because the SZA is small, but also because the total column ozone there is also low compared to higher latitudes.

Commentary appended to the manuscript as '... solar zenith angle and the total column ozone are small.'

P3, L24 I would also cite the two WMO reports addressing the UVI and the 'Global Solar UV Index' publication by the WMO.

Citations added in a new paragraph immediately following equation 3. The bulk of that paragraph was previously in the abstract and moved following a request by the second reviewer to shorten the abstract.

P4, L 6 Is there a reference for the GEM?

Citation of 'Charron et al. (2012), and references therein,' added.

P4, L11 Provide a reference here at the initial mention of the Cloud-J model.

Citation of Prather (2015) added.

P4, L20 Is there a reference for the cccmarad RTM?

Citation of Scinocca et al. (2008) added.

P4, L34 Is the ozone (total and mixing ratios) really generated separately? The next paragraph discusses how LINOZ scheme is used 'within' the GEM to generate ozone forecasts.

Yes, the ozone analyses (ozone mixing ratio analysis fields) were generated separately from the weather analyses. This just means that a separate application of the variational assimilation with GOME-2 ozone data (described in the next paragraph of that section) was applied for ozone relative to the application of variational assimilation with weather data. This was done since the weather analyses had been generated previously. The ozone forecasts are generated by LINOZ within GEM. The process of assimilation improves on these forecast fields at regular time intervals of 6 hours, these improved fields are called analyses and are fed back to the model (to serve as new initial conditions) for it to generate the forecasts for the following time periods. The total column ozone is calculated (also in LINOZ) from vertically integrating the ozone mixing ratio profiles.

P10, L7 Can you determine the elevation adjustment per kilometer to determine if the difference between the grid point elevation and the actual elevation is the reason?

This could be performed but was not done. It is just one factor among many others that could have affected the comparisons and results over the different stations and there was no clear evidence to suggest that it was a comparatively important attribute to this effect. A small change in UV index in the order of roughly 1.5% only is estimated for a difference of 150 m. A related statement has been added to the text.

P10, L7 While doing the above can you determine if the elevation adjustment is equal at all UV wavelengths or wavelength specific?

An adjustment for elevation would require a wavelength specific correction. To demonstrate, the surface pressure was modified in Cloud-J for seven wavelengths in the 280-400 nm range in a given geographical location (Toronto, 29 Aug 2015) to determine the percent difference in the surface irradiance contribution for each of the wavelengths at two different surface pressures. Pressures of 995 hPa and 1013 hPa were used, which correspond to an altitude difference of ∼150 m. The percent differences in irradiance are as follows: 280 nm (1.55%), 300 nm (1.05%), 320 nm (0.68%), 340 nm (0.54%), 360 nm (0.45%), 380 nm (0.38%), 400 nm (0.32%). In all, a disparity in altitude of up to 150 m would generate an error no greater than ∼1.5%.

P10, L12 Is there a plan to bias adjust the GOME observations to bring them more in line with the Brewer observations?

Yes. That work has been done (using another satellite data source that is in better agreement with Brewers) and is the topic of a separate journal paper to be submitted.

P12, L4 Typing error : "Simpson's rule"

Text Corrected.

P12, L15 Do you plan to 'correct' the GEM equivalent broadband absorption cross-section and the TOA solar fluxes to agree with the Cloud-J?

We only plan to scale the GEM broadband irradiances to emulate the general tendency of Cloud-J output as a function of the irradiance value as done in this paper and indicated at the end of Section 3.1.1. This takes the position that the OMI TOA solar spectrum in Cloud-J are deemed 'correct'. The sample effective broadband cross-section value was derived for irradiances at the surface and would not be valid for other levels (nor necessarily all differing ozone profiles). As well, choosing to revisit or not the TOA solar fluxes (and or the applied cross-sections) would be the prerogative of those responsible for the model.

P13, L20 All of these adjustments or scalings will need to be revisited every time the GEM's radiation code is modified. Communication and collaboration between the authors and the GEM modelers needs to be strong such that these differences can be addressed and best corrected in the GEM so that the number of adjustments in the UVI computations is limited or eliminated.

Yes, should there ever be future pertinent modifications to the GEM radiation code, adjustments to the scalings and fits for UV Index determination would have to be made or considered depending on the significance of the change. We do not anticipate our work affecting the GEM radiation code development as such. A suite of programs has been created with a users' manual so that other collaborators/modelers can rerun the programs using updated GEM output files containing data using a newer/modified radiation scheme so new sets of scaling functions can be generated and the broadbands re-weighted accordingly.

P13, L31 The I294-310 is where the bulk of the erythemal weighted values come from. I would think that the coefficient (11.03) would be total column ozone and solar zenith angle dependent.

Considering Figure 9 and the related results, it was a pleasant surprise that constant scaling factors were sufficient for that equation to provide good UV Index values (e.g. errors/differences in UV Index of typically still within 0.2-0.3 with some exceptions), this in light of the erythemal weight varying significantly with wavelength for the two central bands. So the dependence of the UV Index on SZA and ozone with this equation is sufficiently well captured through only the broadband irradiances themselves - as the calculation of broadband irradiances is dependent on SZA and the ozone profile (and, as such, total column ozone).

P14, L18 I presume that the actual total column ozone was used during this comparison and not the OMI climatology, then why wasn't the GEM's albedo used instead of the OMI albedo climatology? Does the GEM's albedo need to be corrected to the OMIs for 100% snow cover? Using the GEM's albedo would then eliminate the 'cold spot' discussed in the following paragraph. The purpose of these two difference plots should be to show the differences between the integrated and linear solutions, not the differences between each and the GEM.

The OMI albedo climatology was used because, with it, wavelength specific global fields for surface reflectivity could be used by Cloud-J to perform the high spectral resolution irradiance calculations. GEM uses a different approach for surface reflectivity where global albedo fields are represented by broadband (UV-NIR) effective values for reflectivity that have been differentiated within the model for specific surface types, of which contain the albedos for soil, glaciers, water, ice, and the aggregated value. For this work, it was therefore deemed more advantageous to use the OMI climatology for our purposes. The resulting larger differences such as in the 'cold spot' would have been removed/reduced using the same albedos. We were willing to accept retaining these differences considering the good agreement of the results elsewhere.

Whether the GEM albedos would need to be corrected to (or account for) the OMI-based values for 100% snow cover would then be the prerogative of the GEM model developers.

We think the purpose of the Fig. 9 needs to cover both aspects (differences with GEM-based values and differences between the methods). While this is implied at the beginning of the second paragraph of Section 3.1.2, a sentence has been added to mention that the integration approach fairs a bit better, i.e. 'The integration approach provides better agreement to Cloud-J, this by up to about 0.1-0.2 for some locations.'

P15, L8 What is meant by 'short term forecasts'? 6, 12, 24, 48 hour?

For this particular section, it refers to daytime 7.5 minute time steps (corrected from 12 minutes - a mixup between two forecast setups) covering up to 24 hours. The text at the beginning of this section has been changed to 'GEM model 24-hour forecast output at 7.5 minute intervals over successive twelve hour forecasts'. A similar change has been made in the last sentence of the Fig. 11 caption. In the section the data spanned solar zenith angles from morning to night. Other references to 'model short-term forecasts' in this section were changed to 'model output'.

P15, L30 Instead of just using the 18 UTC observations and model output, other times of the day could have been used to generate additional UVI and solar zenith angle determinations. Additionally, the range of total ozone values over Canada during July and August are rather small. Comparisons between model and observations could have also been done for April or May when the sun is relatively not too low in the sky but range of total column ozone values is much greater.

The 18 UTC field alone were used only in the other sections as clarified for the above point. While we did have forecasts relying on assimilated ozone data for the Summer already available, we did not have such forecasts for the Spring.

P16, L31 As % cloud amount increases so does the variability of transmission through the clouds. Such a plot in place of the density plot may better show the differences between the Cloud-J and the GEM all sky values. It would be interesting to note if, via the Cloud-J model, there is a spectral dependence of UV adjustments upon cloud amount, type, altitude. The point of the text discussion is that the GEM and the Cloud-J produce reasonably similar results under all-sky conditions. Is it known whether either is correct against real world observations from the Brewers or solar radiometers?

The purpose of the density plot was to make the point that there were many more occurrences of reasonably good agreement than large disagreements, this not being evident from panel of Figure 12. The previous P16 L32-33 lines were modified to '... along or near the regression line, largely, but not entirely, represent those surface irradiances under cloudless or light-cloud, conditions. The probability of deviation from the regression line typically increases with increasing cloud amount and opaqueness.' This is further illustrated by Figure 13 which shows the reduced agreement with increasing ECC (cloud fraction X (1- cloud transmittance)). The last sentence of that paragraph was not clear and out of place. It has been moved following the next paragraph introducing Figure 13 and clarified.

A plot of cloud amount itself versus variability (and or differences) of transmission through the clouds would provide a demonstration of the difficulty of correlating cloud amount alone to the impact of clouds on the UV Index - at least when cloud amounts are not that small, e.g. $\gtrapprox$30-50%. While we prefer not embarking on this for this paper, it is worth considering in further examining/qualifying the impact of clouds (and model clouds) on the UV Index.

It should be noted that the Cloud-J calculations do take into consideration cloud scattering and absorption that is wavelength dependent and also accounts for water droplet size and ice crystal type. Values are provided through the use of look-up tables.

We have not evaluated the accuracy of the model clouds in their resulting impact, characteristics, and coincidence of occurence relative to ground-based measurements (or even satellite base cloud measurements). We do not known the level of correctness of either cloud models. This is something of interest that is beyond the scope of this study.

P18, L10 I gather this answers my previous question about spectral impacts upon cloud amount. Or else the impacts are accumulated in the band coefficients.

The CloudJ calculations for cloud scattering and absorption are wavelength dependent using interpolated data obtained from look-up table parameters for water droplet size and ice crystal type.

P18, L22 There are only so many aspects of solar radiation that can be accounted for. Hopefully, these additional aspects are second order and fall within the error bars of the UVI values.

Hopefully, these geometry considerations do fall within the current uncertainty levels associated to the representation of spatially extended overhead clouds and their impact on the UV index. The treatment of water/ice clouds, particularly for non-uniform opacity and scattering within clouds, is one of the most challenging aspects to correctly manage within radiative transfer models.

Figure 11 The symbols and line need to be identified in the figure caption. The Y axis caption also needs to have '% difference' in it.

Correction made.

Figure 13 Add 'effective' to cloud cover (ECC) in first line of figure caption.

Correction made.

# Responses to Anonymous Referee #2

Interactive comments on:

**Optimizing UV index determination from broadband irradiances**
**by**
**Keith A. Tereszchuk et al.**

Provided by: Anonymous Referee #2
Received and published: 27 January 2018

Preamble: In addition to the changes made to the manuscript following the suggestions of the two reviewers, we also identified three minor issues that required performing a re-analysis of the data and also modifying comments regarding the comparison to Brewer measurements of Section 2.2. These changes did result in a small correction in the scaling and fit factors, but results remain essentially the same (other than improving the agreement with Brewer UV irradiances). These points are as follows:

1. An adjustment of the broadband wavelength boundaries from 280, 294, 310, and 400 nm to 280.11, 294.12, 310.70, and 400.00 nm (this was an error)
2. A correction in applying a moving boxcar averaging window covering ±0.25 nm about sampling points at intervals of 0.5 nm
3. A correction in the calculation of differences with the Brewer UV spectra in Section 2.2, resulting, most significantly, in a reduction of the mean percent differences for the 311-330 nm band from 7.5% to 2.9% (and implying related text changes).

The correction of few other typographical errors were also made.

Page 1 Row 1: In its current form, the abstract is quite long. The reader would appreciate a more concise abstract where the main objectives and major findings are summarized.

The abstract has been made more succinct.

Page 3 Row 3: As regards the action spectrum for erythema, which is the basis for the UV Index, you refer to McKinlay&Diffey (1987) and CIE Technical Report (2014). However, Eq. (1) does not exactly comply with either of these. In the formulation given by McKinlay&Diffey (1987), there are no "smaller than" ("<") signs, only "smaller than or equal" ("$\leq$") signs. This would cause a small jump at 328 nm - which you do not have in your curve in Fig. 1, so probably you are not using the action spectrum of McKinlay&Diffey (1987). CIE Technical Report (2014) refers to ISO/CIE1999 and gives a piecewise function where the signs are like in your Eq. (1). However, the equation for the range 328 < lambda < 400 includes a term (140 − lambda), not (139 − lambda) in the exponent, as does your Eq. (1). Please check which erythemally weighted action spectrum you are using and give a reference for that. An excellent description on the differences between the different erythemally weighted action spectra may be found, for instance, in Webb et al. (2011).

Reference: Webb, A.R., Slaper, H., Koepke, P. & Schmalwieser, A.W. 2011. Know your standard: clarifying the CIE erythema action spectrum. Photochemistry and Photobiology 87: 483-486.

The erythmal action spectrum that was originally intended to be used was the McKinlay&Diffey (1987) reference spectrum. This spectrum had been reported in a number of publications in the literature search of the UV Index as the benchmark erythemal spectrum to be used in the calcualtion of the UV Index. Ultimately, the piece-wise function that was actually used was the one detailed in a NOAA reference article found here:

http://www.esrl.noaa.gov/gmd/grad/neubrew/docs/UVindex.pdf

The article cites their representation of the erythmal action function as being the one published by McKinlay&Diffey (1987). It appears that the NOAA article contains a typo in the wavelength limits that had not been noticed.

The UV calculations in this work and associated figures for the manuscript have been redone using the action spectrum detailled in the CIE Technical Report (2014). The jump referred to at 328 nm is present in the original Fig. 1 plot, but is not large enough to be discernible. The manuscript has been edited to explain the change in the function and reference has been made to the Webb et al. (2011) publication.

Page 4 Line 1: You refer to Long (2003) in the context of UV Index forecasting practices worldwide. More recently, Schmalwieser et al. (2017) has also reported on UV Index monitoring practices in Europe. That work could be also worth referring to.

Reference: Schmalwieser, A.W., Grobner, J., Blumthaler, M., Klotz, B., De Backer, H., Bolsee, D., Werner, R., Tomsic, D., Metelka, L., Eriksen, P., Jepsen, N., Aun, M., Heikkila, A., Duprat, T., Sandmann, H., Weiss, T., Bais, A., Toth, Z., Siani, A., Vaccaro, L., Diemoz, H., Grifoni, D., Zipoli, G., Lorenzetto, G., Petkov, B.H., di Sarra, A.G., Massen, F., Yousif, C., Aculinin, A.A., den Outer, P., Svendby, T., Dahlback, A., Johnsen, B., Biszczuk-Jakubowska, J., Krzyscin, J., Henriques, D., Chubarova, N., Kolarz, P., Mijatovic, Z., Groselj, D., Pribullova, A., Gonzales, J.R.M., Bilbao, J., Guerrero, J.M.V., Serrano, A., Andersson, S., Vuilleumier, L., Webb, A. & O'Hagan, J. 2017. UV Index monitoring in Europe. Photochemical & Photobiological Sciences 16: 1349-1370.

Citation added.

Page 4 Line 26: "the total (clear+cloudy) sky analog". It is not very clear to this reader what this means. Could you please rephrase?

Clarification made to manuscript.

Page 9 Line 6: You have chosen to use weekly (7-day) averages. Could you please explain to the reader why you have chosen averages calculated for a period of 7 days? Why not 5 days – or 10 days?

While the choice of seven days was arbitrary as fewer or more days could also have been selected, the averaging was done for computational efficiency in the minimization. This text has been added to the manuscript.

Page 9 Line 24: You examine 5-day averages of Brewer measurements. Could you please justify the use of 5-day averages? Why not 7-day averages here?

Again arbitary. It was also partially limited by the number of coincident Brewer measurements, made under clear sky conditions, which were recorded within ∼2 minutes local time of the analogous model data produced for the July-August 2015 period. This has been added in the manuscript.

Page 9 Line 23. You remind the reader that a boxcar averaging window was used for the OMI composite TOA spectrum and point out that the slit function of a Brewer spectrophotometer is trapezoid-shaped. The Brewer spectra can be purged from the effects of the slit function by performing a deconvolution. Could you please briefly discuss on how much the different schemes, averaging with a boxcar window vs. convolution with a triangular slit function, may be estimated to affect to the spectra.

Before proceeding, it is necessary to point out that the text should have referred to an approximately triangular-shaped slit function (not trapezoid-shaped). The text has been corrected. Deconvolving the Brewer spectra could have been performed for the model v. instrument comparison, but would have been an involved process. This not only in considering the Brewer slit function, but also in accounting for the spectral variability present in the

TOA solar spectrum in the process. An alternative would have been to apply a triangle-shape averaging function to the TOA spectrum for the simulations instead of the boxcar approach. This would have shown the difference in implications of the two averaging approaches. Notable disparities are visually observed at relative extrema points in some of the plots seen in Fig. 4, suggesting that the differences of averaging functions may play a notable role in these disparities. We preferred not doing this as the overall consistency in spectral shape between the simulated and measured data is sufficient for this work. Note that the text of that section has also been revised due to improvements/corrections in the calculations as pointed out at the beginning of this document.

In addition, it was desired to focus on the re-processing and regenerating the figures and updating the text following the corrections identified above in the preamble (and the adjustment of the applied erythemal action spectrum indicated above).

Page 16 Line 2: “The simulated broadbands”. I think it should be “The simulated broadband irradiances”. There are some other instances in the body text with the same kind of formulation where the actual physical quantity is missing, like on Page 16 Line 28: “all sky broadbands” or Page 14 Line 8: “GEM broadbands”. Please add the name of the physical quantity wherever it is currently missing.

Corrections made. ‘All sky’ has also been changed to ‘all-sky’ for consistency with use of ‘clear-sky’.

Page 17 Line 33: What is a “spectral broadband”? Please explain the term.

The coarse spectral resolution GEM irradiance broadbands. The explanation has been added to the manuscript.

Page 18 (Conclusions). The reader would be extremely interested in any estimate on how much your approach would save computer time as compared to the current operational UV index forecasting. Would you please be able to give an estimate on that?

Neglecting the limitation of the current operational UV index forecasting in providing good UV Index values essentially only over parts of Canada and the northern U.S. (the new setup allows for global coverage at whatever model resolution is available), there are two phases to consider. One is providing the ozone field and or the GEM weather variable or irradiance fields. The second is the calculation of the UV Index itself from the ozone and GEM model output.

The first phase of the two methods are quite different. The operational approach first requires the calculation of total column ozone from weather fields over a pre-determined northern hemisphere grid. On the other hand the setup in this paper requires that ozone field assimilation and forecasting be performed first. This by itself would be much more computationally expensive. On the other hand, the ozone assimilation and forecasting process is also intended to benefit other applications. The ozone field forecast is then provided, instead of an ozone climatology, to the model radiation code applied for weather forecasting and so does not add any cost.

For this second phase, it is not believed there would be much or any computational advantage. The calculation for this new setup requires the scaling of the GEM UV surface broadband total irradiances and their application in the integration or linear interpolation approaches. Considering the equations involved, the linear interpolation approach might be a faster and the integration approach could be similar if not a bit slower. The integration was still made to be computationally quite efficient. A few repeat UV Index calculation runs of $\sim$11500 points for each case required, on average, $\sim$0.08 seconds for the operational case and the integration approach and about $\sim$0.07 seconds for the linear interpolation (assuming the units are correct for the conversion of processor clock counts to seconds), with some calculations performed being common to all three cases. This phase of the calculations does not imply any significant time as compared to model forecasting (and estimating the total column ozone for the operational case.

# Optimizing UV ~~index~~ Index determination from broadband irradiances

**Keith. A. Tereszchuk**[1], **Yves. J. Rochon**[1], **Chris. A. McLinden**[1], **and Paul. A. Vaillancourt**[2]

[1]Air Quality Research Division, Environment and Climate Change Canada, Toronto, Ontario, Canada
[2]Meteorological Research Division, Environment and Climate Change Canada, Dorval, Quebec, Canada

*Correspondence to:* Keith A. Tereszchuk (keith.tereszchuk@canada.ca)
Yves J. Rochon (yves.rochon@canada.ca)

**Abstract.** ~~Amidst mounting concerns about the depletion of stratospheric ozone ($O_3$), and for subsequent increases in the surface irradiances of ultraviolet (UV) light and its effects on human health, a daily UV forecast program was launched by Environment Canada in 1993. The program serves to monitor harmful surface UV radiation and provide this information to the Canadian public through the UV index, a scale which reports the relative intensity of the Sun's UV radiation at the Earth's surface, and the corresponding protection actions to be taken. The UV index was accepted as a standard method of reporting surface UV irradiances by the World Meteorological Organization (WMO) and World Health Organization (WHO) in 1994.~~

A study was undertaken to improve upon the prognosticative capability of Environment and Climate Change Canada's (ECCC) UV ~~index~~ Index forecast model. An aspect of that work, and the topic of this communication, was to investigate the use of the four UV broadband surface irradiance fields generated by ECCC's Global Environmental Multiscale (GEM) numerical prediction model to determine the UV ~~index~~Index.

The basis of the investigation involves the creation of a suite of routines which employ high spectral resolution radiative transfer code developed to calculate UV ~~index~~ Index fields from GEM forecasts. These routines employ a modified version of the Cloud-J v7.4 radiative transfer model, which integrates GEM output to produce high spectral resolution surface irradiance fields. The output generated using the high-resolution radiative transfer code served to verify and calibrate GEM broadband surface irradiances under clear-sky conditions and their use in providing the UV ~~index~~Index. A subsequent comparison of irradiances and UV ~~index~~ Index under cloudy conditions was also performed.

Linear correlation agreement of surface irradiances from the two models for each of the two higher UV bands covering ~~310-330 nm and 330-400~~ 310.70-330.03 nm and 330.03-400.00 nm is typically greater than 95% for clear-sky conditions with associated root mean square relative errors of ~~5.5% and 3.8~~6.4% and 4.0%. On the other hand, underestimations of clear-sky GEM irradiances were found on the order of ∼30-50% for the ~~294-310~~ 294.12-310.70 nm band and by a factor of ∼30 for the ~~280-294~~ 280.11-294.12 nm band. This underestimation can be significant for UV ~~index~~ Index determination but would not impact weather forecasting. Corresponding empirical adjustments were applied to the broadband irradiances now giving a correlation coefficient of unity. From these, a least-squares fitting was derived for the calculation of the UV ~~index~~Index. The resultant differences in UV indices from the high spectral resolution irradiances and the resultant GEM broadband irradiances are typically within 0.2-0.3 with a root mean square relative error in the scatter of ∼~~5.5~~6.6% for clear-sky conditions. Similar results are reproduced under cloudy conditions with light to moderate clouds, having a relative error comparable to the clear-sky counterpart; under strong attenuation due to clouds, a substantial increase in the root mean square relative error of up to ~~30~~35% is observed due to differing cloud radiative transfer models.

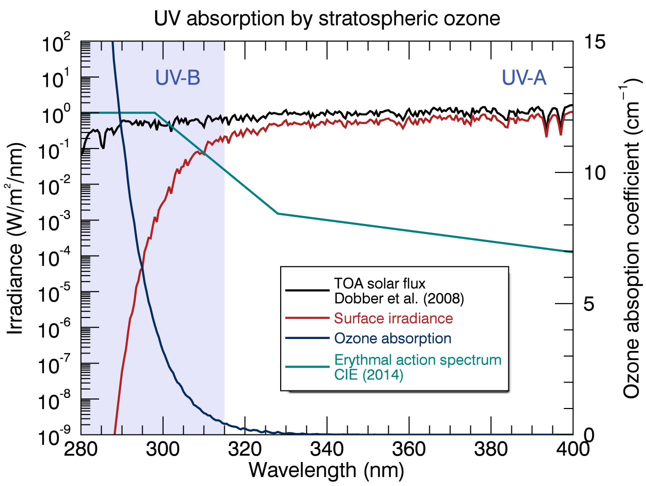


**Figure 1.** Sample UV irradiance spectrum at the Earth's surface on a clear summer day (averaged and sampled over 0.5 nm intervals). Stratospheric ($O_3$) is the primary species which serves to absorb UV radiation in the atmosphere (blue curve). The Huggins/Hartley band system of $O_3$ attenuates the radiative flux (black curve) by several orders of magnitude in the UV-B region. The product of the absorption cross-section and the top-of-atmosphere flux gives the resultant incoming irradiance at the surface (red curve). The erythemal action spectrum (green curve), demonstrates the increasing susceptibility of human skin to epidermal damage (erythema).



## 1 Introduction

Throughout the late 1980s and early 1990s, extensive atmospheric studies in the polar regions of the planet revealed that stratospheric ozone ($O_3$) concentrations were being depleted due to a variety of $O_3$ destroying catalytic cycles driven by photochemical reactions liberating chlorine (Cl) and bromine (Br) atoms from chlorofluorocarbon (CFC) and hydrofluorocarbon (HCFC) molecules emitted into the atmosphere as airborne anthropogenic pollutants (Rowland , 1996).

Ozone is an important atmospheric absorber of energetic, short-wavelength, radiation emitted by the Sun. Most critically, $O_3$ is the primary absorber of ultraviolet (UV) radiation, which has wide-ranging implications on the health of the biosphere; both on a molecular level with the potential of damaging the cellular DNA of individual organisms (Ravanat et al. , 2001), to the destabilization of entire biogeochemical cycles within a biome (Zepp et al. , 1998).

UV radiation is categorized into three broadband regions which are defined as: UV-A (315-400 nm), UV-B (280-315 nm) and UV-C (100-280 nm). Molecular species in the Earth's atmosphere absorb very little of the longer wavelength UV-A radiation, as it reaches the surface with a minor net difference (mainly due to scattering) in the radiative flux from the top of the atmosphere. UV-B radiation is partially transmitted through the atmosphere and is primarily absorbed by $O_3$ (Huggins/Hartley band system). The Huggins/Hartley system (∼200-360 nm) of $O_3$ and the Hopfield/~~Schumann?Runge~~ Schumann–Runge system (∼70-200 nm) of molecular oxygen ($O_2$) serve to absorb all UV-C radiation, which is impeded from reaching the top of the troposphere. This absorption occurs primarily in the ozone layer, a thin band of $O_3$ contained within the stratosphere where the peak molecular number density of $O_3$ is located ∼20-30 km above sea level. Figure 1 demonstrates how the absorption by ozone increases rapidly with decreasing wavelength in the UV-B region, causing surface irradiances to fall off sharply with decreasing wavelength.

At progressively shorter wavelengths of UV light, increasingly energetic photons become subsequently more and more damaging to biological species, including humans. Studies were conducted as early as the 1930s to quantify the damage done to human skin by UV radiation. It had been well known for quite some time that UV-A and UV-B radiation is harmful to unicellular organisms, the surface cells of plants and animals, and to the health of the more ~~sensitive population.~~ photosensitive population. Increased photosensitivity in people can be caused by a number factors, the most common cause is due to having minimal skin pigmentation (melanin), which provides a natural barrier to the Sun's UV rays. Certain immune system ailments such as solar urticaria can cause hypersensitive allergic reactions to minimal exposures of UV radiation causing hives, rashes, and blistering. Photosensitivity is often associated with the use of certain medications, including some non-steroidal anti-inflammatory drugs and painkillers, tranquillizers, oral anti-diabetics, antibiotics and antidepressants (http://www.who.int/uv/faq/uvhealtfac/en/).

Colblentz and Stair (1934) sought to obtain measurements of the spectral erythemic reaction (reddening) of untanned human skin exposed to UV light. In essence, this was one of the first recordings of a UV erythemal action spectrum, where an action spectrum for a particular biological effect expresses the effectiveness of radiation at each wavelength as a fraction of the effectiveness at a certain standard wavelength. In this case, the tolerance of human skin to ultraviolet radiation. Today, research has revealed that humans are susceptible to much more than sunburns when exposed to UV rays. Prolonged exposure can lead to the premature aging of the skin, suppression of the immune system, eye damage including the development of corneal photokeratitis and cataracts, and skin cancer (melanoma). The contemporary action spectrum adopted by most international organizations is the CIE (Commission Internationale de l'Éclairage, International Commission on Illumination) action spectrum ~~using the method outlined by McKinlay and Diffey (1987); CIE Technical Report (2014). The piecewise function in~~ (CIE Technical Report , 2014). The CIE standard spectrum, Eq. (**??**), ~~which mathematically~~

~~represents the McKinlay-Diffey erythemal action spectrum , is also detailed in Fig. 1~~is based on the action spectrum originally developed by McKinlay and Diffey (1987), which was constructed by re-normalizing the data points and modifying the piecewise function to avoid having overlapping wavelength intervals (Webb et al. , 2011).

$$EAS(\lambda) = \{$$

The UV ~~index~~ Index was developed as an erythemally weighted representation of the total surface flux of UV radiation in the biologically active range of 280-400 nm (CIE Technical Report , 2014; Fioletov et al. , 1997; Allaart et al. , 2004; Fioletov et al. , 2010; Moshammer et al. , 2016); the range below ∼280-290 nm can be excluded as its contribution is negligible. It was conceived to produce a simplified scale which reports the relative strength of the Sun's UV radiation, and to inform the public of the Sun protection actions that should be taken as a precaution if they are to be exposed to the Sun's rays for extended periods of time.

To determine the UV ~~index~~ Index from high spectral resolution irradiances, an effective spectral curve is calculated from the product of the erythemal action spectrum and the surface irradiance (Fig. 2). This effective curve, the weighted UV irradiance, is then integrated over the spectral range representing the UV-A and UV-B (280-400 nm) to produce the UV ~~index~~ Index (see Eq. (2)). A scaling factor of $(25\mathrm{mW/m^2})^{-1}$ is implemented to provide a convenient set of ~~integer~~ numerical values, normally ranging from 0 to 11. In extreme cases, values of >11 can be reached and are typically recorded in the tropics where the solar zenith angle ~~is at a minimum~~and the total column ozone are small. Extreme values are also recorded at high elevations where the atmospheric optical path is shortened, resulting in a reduced attenuation of actinic fluxes and consequently producing increased surface irradiances.

$$UVI = \frac{1}{25\,\frac{\mathrm{mW}}{\mathrm{m}^2}} \int_{280\,\mathrm{nm}}^{400\,\mathrm{nm}} I(\lambda)\cdot EAS(\lambda)\,\mathrm{d}\lambda \qquad (2)$$

~~Following~~ Amidst mounting concerns arising in the late 1980s from the escalating ~~loss~~ depletion of stratospheric $O_3$ due to CFCs, and the subsequent increases in the surface irradiances of UV radiation (Crutzen , 1992), Environment and Climate Change Canada began providing daily UV ~~index~~ Index forecasts as of 1992 (Burrows et al. , 1994). Since its inception in 1992, the UV ~~index~~ Index has been adopted worldwide as standard indicator to characterize solar UV intensity at the Earth's surface (Fioletov et al. , 2010) and serves to inform the public about the strength of the Sun's UV radiation and the adequate sun protection actions recommended to avoid excessive exposure to UV radiation ~~.~~ (WHO Report , 2002; CIE Technical Report , 2014). The UV Index was officially adopted as the method of reporting surface UV irradiances by the World Meteorological Organization (WMO) and World Health Organization (WHO) in 1994.

At present, the UV ~~index~~ Index determination for the ECCC forecast system relies on a statistically derived weather-based computation of the total column ozone field, adjustments using total column measurements of the Canadian Brewer network and empirical conversions to the UV ~~index~~ Index accounting for the solar zenith angle, cloud conditions, surface altitude and snow cover. A recently undertaken study toward improving the UV ~~index~~ Index forecast system makes direct use of ozone data assimilation, ozone model forecasts, and model UV irradiance forecasts for both clear-sky and cloudy conditions as done in some capacity at other forecast centers (e.g., NCEP/NOAA, KNMI, and ECMWF). A summary of UV ~~index~~ Index forecasting practices conducted by various governmental organizations worldwide were compiled by Long (2003); a more recently updated overview of UV measurement stations and monitoring networks in Europe was reported by Schmalwieser et al. (2017).

This current study is part of a multi-faceted project which seeks to include having a UV ~~index~~ Index forecasting package more tightly integrated into the current weather (and air quality) forecasting system, and increasing the array of UV ~~index~~ Index products available from ECCC to Canadians, such as daytime variation, longer forecasts, and continental and regional maps. The ECCC Global Environmental Multiscale (GEM) numerical weather prediction model described by Charron et al. (2012), and the references therein, provides four broadband irradiances shown in Fig. 2 covering the UV spectrum in the range of 280-400 nm, which can be calculated using three-dimensional prognostic ozone fields. The work presented in this communication consists of investigating and optimizing the calculation of the UV ~~index~~ Index from these broadband irradiances, with focus on clear-sky conditions, for minimizing computational cost and processing time. This is done through comparisons of the UV ~~index~~ Index and broadbands irradiances produced from GEM to those calculated using the Cloud-J radiative transfer model (Prather , 2015), which has been adapted to provide high resolution irradiance spectra at the Earth's surface.

The following subsections provide some background on the GEM-based weather forecast system, the Cloud-J radiative transfer model, and their products. Section 2 describes the general methodology and the related fitting approaches applied in Sect. 3 to investigate and optimize the calculation of the UV ~~index~~ Index from the broadband irradiances through the use of high-resolution spectral irradiance simulations for clear-sky conditions. While a specific optimization under cloudy conditions is not performed due to differing cloud radiative transfer models, comparisons for both clear and cloudy conditions are presented and fully discussed in Sect. 3. Conclusions are provided in Sect. 4.

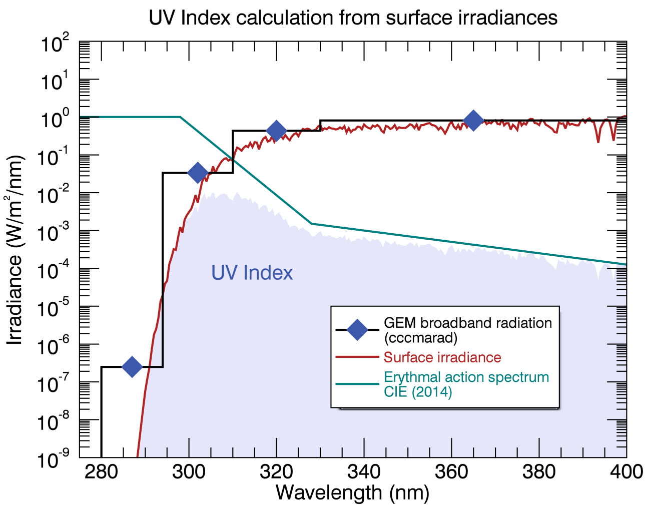


**Figure 2.** The UV ~~index~~ Index is defined as the integral of the erythemally weighted irradiance spectrum (shaded region), produced from the product of the surface irradiance (red curve; see Fig. 1) and the erythemal action spectrum (green curve), over the UV-A and UV-B spectral range. The result is then multiplied by a scaling factor (25 mW/m$^2$)$^{-1}$ to create a numerically convenient value for the index. Also depicted are the corresponding irradiances for the GEM broadbands divided by their respective bandwidths.

### 1.1 GEM with LINOZ

The irradiance fields calculated by GEM ~~are based on the cccmarad radiative transfer scheme~~ use the CCCmarad radiative transfer model. CCCmarad is an in-house radiation scheme based on a modified version of the Canadian Centre for Climate Modelling and Analysis (CCCma) atmospheric general circulation model (Scinocca et al. , 2008), which uses a correlated-k distribution method for gaseous transmission detailed by Li and Barker (2005) and von Salzen et al. (2013). The Li and Barker (2005) radiation scheme has four wavenumber intervals for the shortwave and nine intervals for the longwave. The visible and UV portion of the shortwave is further subdivided into 9 subbands. The four subbands of relevance to the calculation of the UV ~~index~~ Index cover the following spectral ranges: ~~280-294 nm, 294-310 nm, 310-330 nm, 330-400~~ 280.11-294.12 nm, 294.12-310.70 nm, 310.70-330.03 nm, 330.03-400.00 nm. For convenience, the remainder of the text, will instead refer to the integer values of 280, 294, 311, and 400 nm. The irradiances of the subbands, i.e., the broadband irradiances, consist of direct and diffuse components which are available in addition to their sum. ~~Also differentiated, are the clear sky and the total (clear+cloudy) sky analog for the total surface irradiance, as well as differentiation for each of the individual direct and diffuse components of the subbands~~This paper involves use of all three irradiance terms of these four subbands. As well, it will separately consider the clear-sky and all-sky cases in the calculation of the irradiances, all-sky conditions implying the possible presence of clouds.

The GEM dynamical core is described in Girard et al. (2014), while basic descriptions of the physical parameterizations or detailed references can be found in Zadra et al. (2014a, b). Model runs were performed using a 7.5 minute time step for a uniform 1024x800 longitude-latitude grid (0.352°x0.225°) and a Charney-Phillips vertically staggered grid with 80 thermodynamic levels extending from the near-surface (at $\eta = 1$) to $\sim$0.1 mbar ($\eta \approx 0.0001$). The analyses, serving as initial conditions for providing the forecasts used in this study, are a composite of the already available ECCC weather analysis and separately generated ozone analyses. The GEM forecast products used as input for the simulations performed with Cloud-J are detailed in Sect. 2.1.

Prognostic ozone is solved with a linearized photochemistry scheme called LINOZ (McLinden et al. , 2000), which was implemented on-line within the GEM NWP model (de Grandpré et al. , 2016). For this work, the ozone analyses stem from assimilation of total column ozone data obtained from the National Environmental Satellite, Data, and Information Service (NESDIS/NOAA) for the Global Ozone Monitoring Experiment-2 (GOME-2) instruments of the MetOp-A and MetOp-B satellites (Callies et al. , 2000; Munro et al. , 2006) . Assimilations were performed with the incremental three-dimensional variational approach with the first guess at appropriate time (FGAT; Fisher and Andersson (2001)) using elements of the system described in Charron et al. (2012), and the references therein, adapted for chemical data assimilation.

For the treatment of cloud, GEM employs a prognostic total cloud water variable with a bulk-microphysics scheme for non-convective clouds. The radiative transfer impact from clouds is primarily dictated by the liquid and ice water mixing ratios (LWCR and IWCR) and cloud fraction (CLDR). Fractional cloudiness is based on a relative humidity threshold, which varies in the vertical. Individual cloud layers are assumed to overlap in the vertical using a maximum random cloud overlap (Sundqvist et al. , 1989; Paquin-Ricard et al. , 2010).

The GEM model currently does not assimilate aerosol measurement data. The radiative effects associated with background aerosols are based on a climatology produced by Toon and Pollack (1976). This climatology specifies maximum aerosol loading at the equator and a decrease toward the poles, with different values for continents and oceans. These distributions also include a latitudinal gradient. Aerosols are assumed only to affect the solar absorption properties of the clear-sky atmosphere (Markovic et al. , 2008).

### 1.2 Cloud-J

Cloud-J, a recent release of the Fast-J program (Wild et al. , 2000; Bian and Prather , 2002), is a multi-scattering, eight-stream, radiative transfer model for solar radiation (Prather ,

2015) developed for integration into three dimensional chemical transport models to calculate photolysis rates ($J$ values) in the atmosphere. The version of the program used for this work is Cloud-J v7.4. The program is developed and maintained by M. Prather in the Department of Earth System Science at the University of California, Irvine (http://www.ess.uci.edu/group/prather/scholar_software/cloud-j).

To calculate photolysis rates, the standard Cloud-J code uses 18 interpolated wavelength bins covering a spectral range of 187-599 nm. The integrated radiative transfer model uses a plane parallel atmosphere assumption and a full scattering phase function. Rayleigh and isotropic scattering are taken into consideration. Numerous cloud types and aerosol species of varying sizes are accounted for in the calculations by making use of look-up tables containing the scattering functions for water droplet size, ice crystals of various phases, dust, absorbing soot (black carbon), stratospheric sulfates (background and volcanic) and water haze at 0.1 $\mu$m and 0.4 $\mu$m. Optical depth properties include extinction optical depth, single scatter albedo, and a scattering phase function.

Cloud-J provides numerous options for the treatment of clouds in its radiative transfer calculations. Option 1 is the calculation for clear-skies conditions. ~~Option~~ Options 2&3 are variations of the direct use of the cloud water content, which employs cloud fraction and separate liquid and ice water paths. The remaining five options (4-8) employ different variations in the correlated, overlapping cloud scheme. The approach seeks to represent the fractional cloud cover in the model layers through the calculation of numerous independent cloud atmospheres (ICAs), where each ICA would be either 100% cloudy or clear in each cell of the cloud model layer. This fractional cloud-overlap model serves to determine the layer structure, weighting, and number of ICAs that best represent the actual cloud distribution in the model layers.

## 2 Methodology

Given the availability of realistic three-dimensional prognostic ozone to the GEM numerical weather prediction model through the LINOZ linearized ozone model and ozone data assimilation, it was proposed to make direct use of the four GEM model UV broadband irradiances at the Earth's surface to calculate the UV ~~index~~Index. The Cloud-J radiative transfer model was adapted to provide high spectral resolution surface irradiances in the UV, 280-400 nm. The high resolution output is used to evaluate the GEM broadband irradiances for clear-sky conditions and to optimize the determination of the UV ~~index~~ Index using these coarse resolution spectral broadbands. A comparison of results from the two models under cloudy conditions is also performed in Sect. 3.

To perform the optimization of the GEM ~~broadbands~~broadband irradiances, the desired output from Cloud-J is two-fold:

1. Sets of Cloud-J broadband irradiances generated by integrating portions of the high resolution irradiance spectra to produce simulated versions of the four GEM UV broadbands covering 280-294 nm, ~~294-310 nm, 310-330~~ 294-311 nm, 311-330 nm and 330-400 nm.

2. A global UV ~~index~~ Index field produced by integrating the erythemally weighted high-resolution irradiance spectra over the 280-400 nm spectral range, Eq. (2).

Simulated ~~broadbands~~ broadband irradiances are generated for comparison with the GEM broadband irradiances and, as needed, used to create sets of scaling functions to calibrate the GEM values to the Cloud-J output. The scaled GEM ~~broadbands~~ broadband irradiances are then weighted accordingly such that the global UV ~~index~~ Index field produced using the GEM ~~broadbands~~ broadband irradiances emulates the high resolution UV ~~index~~ Index field calculated from Cloud-J. Two different approaches were implemented to calculate the UV ~~index~~ Index from the resultant GEM broadband surface irradiances. A least-squares fitting was employed in both cases to optimize the weighting under clear-sky conditions using the UV ~~index~~ Index field produced from the high-resolution Cloud-J spectra as a reference.

The following subsections briefly describe the application of GEM products and the Cloud-J model to ultimately evaluate and optimize the UV ~~index~~ Index determination from the broadband irradiances.

### 2.1 Calculation of high spectral resolution irradiances

Originally designed to calculate tropospheric/stratospheric photolysis rates in 3D global models, the Cloud-J program was adapted to input three-dimensional fields from the GEM model and output direct and diffuse, high spectral resolution, surface irradiances instead of mean photolytic intensities. The resultant surface spectral irradiances are, in turn, used to calculate UV ~~index~~ Index fields.

To produce the high spectral resolution output for UV ~~index~~ Index calculations, the number of wavelength bins was increased to 241 with 0.5 nm intervals over the 280-400 nm spectral range. Having augmented the number of wavelength bins to perform the high resolution calculations, additional spectroscopic data was required for integration into Cloud-J. These spectral parameters were interpolated onto a 0.5 nm resolution grid and reformatted for reading into the program along with the GEM model forecasts. The spectral data incorporated into Cloud-J include:

- A set of UV-Visible temperature/pressure absorption cross-sections for $O_3$ obtained from the GEISA spectroscopic database (Jacquinet-Husson et al. , 2008).

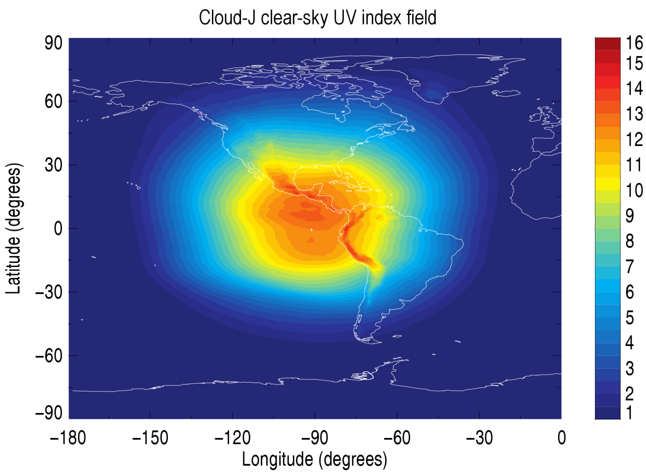


**Figure 3.** Cloud-J clear-sky UV ~~index~~ Index field produced using GEM 6h forecast data with the OMI and GEISA spectral parameters detailed in Sect. 2.1. The UV ~~index~~ Index field was generated from a 7-day average of spectral irradiances produced from 23-29 August 2015 at 18h UTC.

- An Earth surface reflectance climatology from five years (2005-2009) of OMI data (Kleipool et al. , 2008). Surface reflectivities are provided as monthly averages for 23 wavelength channels, 328-499 nm range, on a 0.5°x0.5°grid.

- A high-resolution, top of atmosphere (TOA), solar flux spectrum between 250 and 550 nm (Dobber et al. , 2008). Provided by Q. Kleipool of the Royal Netherlands Meteorological Institute, the reference spectrum was created to calibrate/validate the Ozone Monitoring Instrument (OMI).

- Rayleigh scattering parameters calculated using the methodology detailed in a publication by Chance and Spurr (1997).

The $O_3$ cross-sections obtained from the GEISA database (http://www.pole-ether.fr/ether/pubipsl/GEISA/geisa_crossUV_frame_2011_uk.jsp) were recorded by Voight et al. (2001) on a Bruker IFS 120HR Fourier-transform spectrometer at a spectral resolution of 5.0 $cm^{-1}$). The measurements were performed as a follow up to the cross-sectional data initially recorded by Burrows et al. (1999) on the GOME-FM instrument. The new data sets recorded by Voight et al. (2001) offer precise reference spectra where the spectral accuracy of the data is better than 0.1 $cm^{-1}$ ($\sim$0.5 pm at 230 nm and $\sim$7.2 pm at 850 nm), which was validated by recording visible absorption spectra of gaseous diatomic iodide $I_2$ in a reference cell using the same experimental set-up. The agreement between observed and modelled data was determined to be 1% and better within the 255-310 nm region. Sets of $O_3$ absorption spectra were recorded using total pressures of 100 mbar and 1000 mbar at five different temperatures ranging from 203-293 K. The spectra in the UV range at 100 and 1000 mbar are nearly identical with larger differences at higher wavenumbers. Three $O_3$ absorption spectra from this data set were used for incorporation into Cloud-J (1000 mbar at 293 K, 100 mbar at 246 K and 223 K). The selection of the three spectra was based on consideration of the typical temperature distribution as a function of pressure.

In addition to the $O_3$ temperature cross-sections, the $O^1D$ quantum yields associated with ozone photolysis were also required by the Cloud-J radiative transfer model. Values for the quantum yields were calculated using the prescribed method outlined by Matsumi et al. (2002) for the same three temperatures associated with the GEISA $O_3$ cross-sections.

The albedo data was interpolated from its native grid onto the 1024x800 GEM global grid. A linear interpolation was then performed on the data from the 23 re-gridded wavelength channels to obtain the intermediate albedo global fields corresponding to 0.5 nm intervals over the 328-400 nm spectral range to be subsequently used in the high resolution irradiance calculations. Albedo values for the bins corresponding to the missing wavelength range of 280-328 nm were obtained by linearly interpolating the data between the 328 nm OMI channel and the UV-B values published by Chadyšien and Girgždys (2008). According to the experimental data reported in Table 2 of Chadyšien and Girgždys (2008), snow/ice is the primary reflector of UV-A and UV-B radiation where surface reflectivity for these spectral regions are 94% and 88% respectively, representing a drop in reflectivity of 6.38% in the shorter wavelength region. To emulate the experimental data, the reflectivities for the 328 nm OMI channel were linearly reduced by 6.38% over the 280-328 nm spectral range.

The OMI solar reference spectrum produced by Dobber et al. (2008) was used to provide the TOA solar flux values required for the high-resolution irradiance calculations performed by Cloud-J. Currently, there are no high resolution solar spectra that cover the UV-A and UV-B wavelength ranges. Most UV/Vis TOA spectra are pieced together from different sources in order to provide a continuous, unbroken spectrum. The OMI reference spectrum was created to validate the radiometric calibration of OMI measurements and to monitor potential optical degradation of the instrument. Also a combined spectrum, it was produced by employing the approach used by Chance and Spurr (1997). It merges the balloon spectrum of Hall and Anderson (1991), which covers a shortwave UV region between 200 and 310 nm, with a ground-based spectrum obtained from the McMath-Pierce solar telescope at Kitt Peak National Observatory (Kurucz et al. , 1984). The broadband Kitt Peak spectrum covers a spectral range of 296 and 1200 nm. The final derived spectrum is at 0.01 nm sampling and at 0.025 nm resolution.

This spectrum was chosen for use in this work, from amongst others, because the OMI composite spectrum uses high resolution (0.01 nm) UV measurements made in the

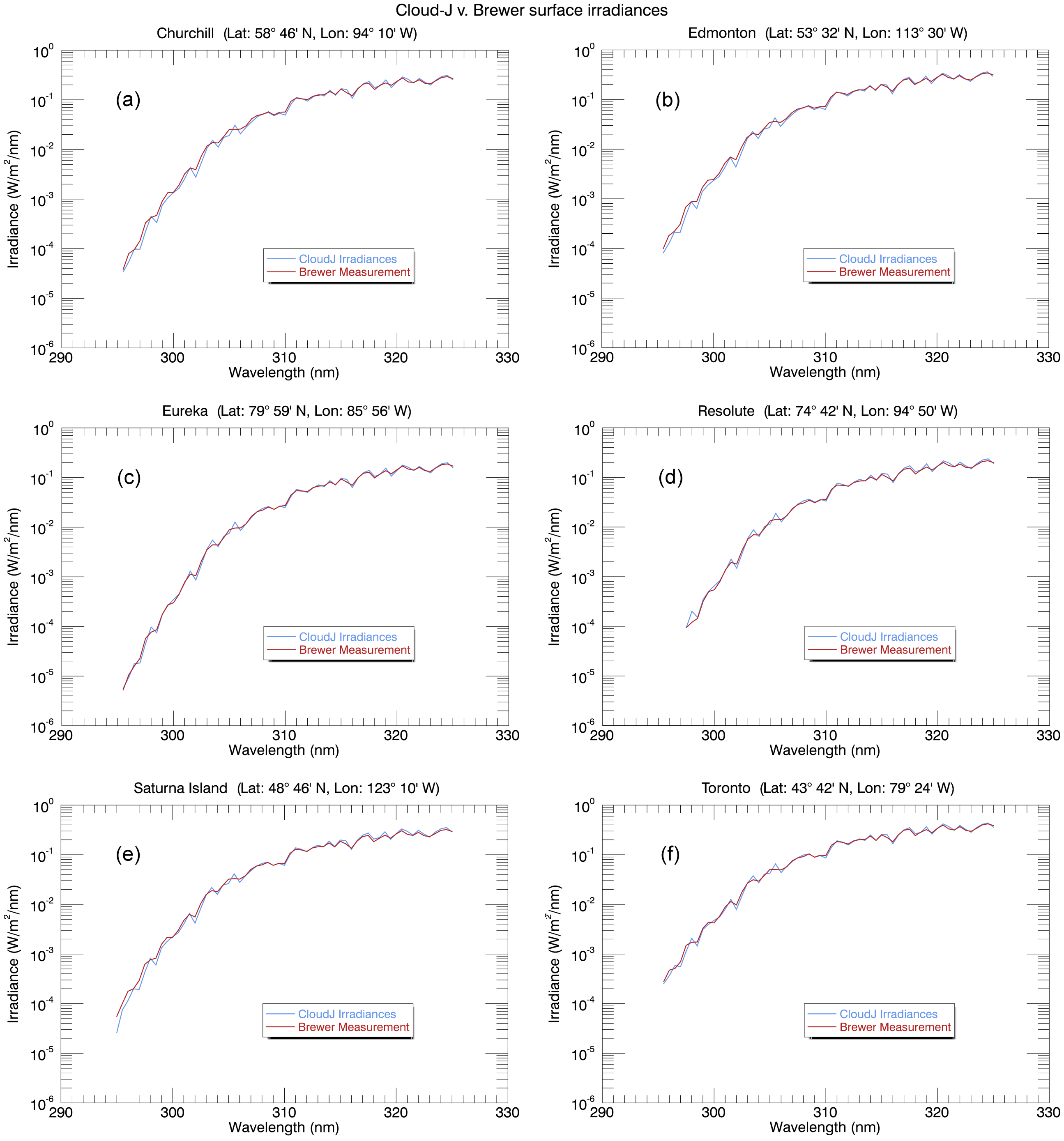


**Figure 4.** Cloud-J clear-sky surface irradiances compared to *in-situ* Brewer measurements obtained from six measurement stations belonging to ECCC's ozone monitoring network. Plotted are 5-day averages for 18h00 UTC of Brewer spectral irradiances (red curve) and the associated Cloud-J irradiances (light blue). The Cloud-J irradiances shown here were calculated with the Dobber et al. (2008) TOA spectrum averaged over 0.5 nm intervals with a sampling resolution also of 0.5 nm.

stratosphere from a balloon at ∼40 km in altitude (Hall and Anderson , 1991) to avoid affects of the strong atmospheric absorption below 300 nm Dobber et al. (2008). The solar reference spectrum produced by Thuillier et al. (2003) was also considered since it is composed from measurements made from the SOLSPEC and SOSP satellite instruments (Thuillier et al. , 1998, 2003) with a resolution of 1 nm. With both spectra being similar, the former was selected due to its

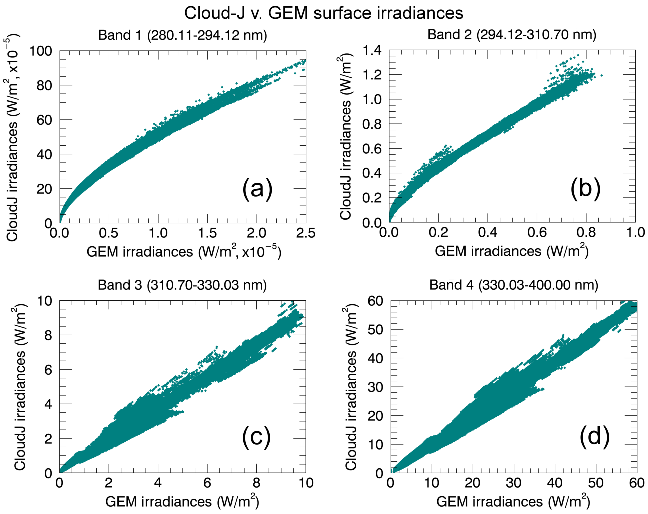


**Figure 5.** Correlation of GEM and Cloud-J total surfaces irradiances for clear-sky conditions. The GEM UV broadband irradiances are compared to simulated broadband irradiances produced by integrating the high resolution Cloud-J output over the same spectral regions. Presented are the individual, 7-day irradiance contributions from 23-29 August 2015.

higher spectral resolution even though the resolution of the latter is only a factor of two coarser than our simulation resolution. A moving boxcar averaging window covering ±0.25 nm about sampling points at intervals of 0.5 nm was applied to the OMI composite spectrum to generate the simulation spectrum.

Consideration was also given to high resolution spectra based on accurate models of the Sun using the Kurucz et al. (1984) spectrum, such as those by Chance and Spurr (1997); Chance and Kurucz (2010), which provide excellent spectral range, sampling, and resolution. These spectra unfortunately neglect optimization in the UV-B region for radiometric accuracy. The SAO96 and re-calibrated SAO96 (SAO2010) reference spectra described by Chance and Kurucz (2010) both utilize the original Kurucz et al. (1984) Kitt Peak spectrum for the UV-B, where $O_3$ structure was not fully removed. Chance and Spurr (1997) reported that efforts were focused on intensity calibration of the wavelength range where most application to satellite measurements are performed. Intensities for portions of the spectrum shortward of 305 nm may be in substantial disagreement, by as much as 20%, with both the Dobber et al. (2008) and Thuillier et al. (2003). These spectra were deemed unsuitable for use in the calculation of the UV ~~index~~Index.

It should be noted that the solar spectrum used in this work is representative of a yearly average value of the Earth's TOA flux. Changes in the Earth-Sun distance and associated solar fluxes during the Earth's annual cycle are taken into account and are corrected for by Cloud-J in the high-resolution simulations.

The input atmospheric conditions provided to Cloud-J for this study consist of a set of 6 hour forecasts from the GEM model output for the dates of August 23-29, 2015, at 18h00 UTC with daytime over North America. The GEM fields provided as input are surface pressure, and the three-dimensional fields of temperature, pressure (derived from the vertical coordinate and surface pressure), ozone, specific humidity (converted to relative humidity), liquid and ice water mixing ratios (LWCR and IWCR), and cloud fraction (CLDR). For the all-sky conditions, the parameters LWCR, IWCR and CLDR determine the liquid and ice water partial column amounts (in g/m$^2$) of each model layer in the presence of clouds.

Cloud-J was run individually for each day during the period of August 23-29 to produce irradiance fields representing the direct, diffuse and total surface flux under both clear-sky and all-sky conditions. Weekly (7-day) averages of the direct, diffuse and total spectral irradiances served as reference spectra in the least-squares minimization for evaluation and adjustments of GEM broadband irradiances, with individual forecast values used in the scatter plot comparisons. While the choice of seven days was arbitrary as fewer or more days could also have been selected, the averaging was done for computational efficiency in the minimization. The UV indices produced with Eq. (2) from the weekly averages of total spectral irradiances served as reference in optimizing of UV ~~index~~ Index estimation models based broadband irradiances. The UV ~~index~~ Index field from the clear-sky weekly averages is shown in Fig. 3.

### 2.2 Comparison to ground-based clear-sky irradiances

In addition to measuring total column ozone, Brewer spectrophotometers provide ground-based measurements of the UV spectrum in the range 290-325 nm with ~~an effective resolution of about 0.55~~ a full-width at half-maximum of about 0.58 nm and a sampling interval of 0.5 nm. The data processing scheme used to generate spectral irradiances at each 0.5 nm interval, which includes calibration and corrections for various factors, is described in the work detailed by Kerr (2010) and the references within. A sample inter-comparison of three Brewer instruments by Thompson et al. (1997) (see Kerr (2010) for other inter-comparison sources) showed relative overall differences between instruments within 6% with an average of 3% for wavelengths longer than 300 nm; uncertainties are larger at shorter wavelengths.

Cloud-J clear-sky surface UV irradiances were compared to Brewer spectra obtained from six different measurement stations belonging to ECCC's ozone monitoring network and identified to be under clear-sky to optically thin cloud conditions. The applied TOA solar spectrum used here for the Cloud-J simulations, as well as for optimizing use of the GEM broadband irradiances in UV ~~index~~ Index calculations, has the same sampling interval of 0.5 nm as

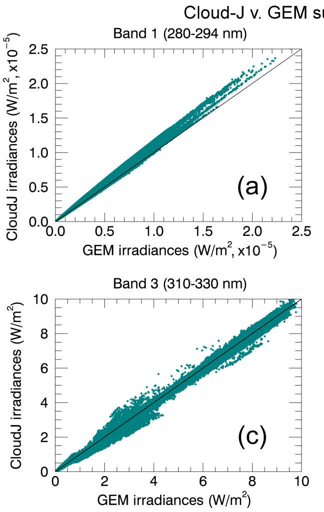


**Figure 6.** ~~Correlation of~~ GEM ~~and Cloud-J total surfaces~~ broadband surface irradiances ~~for clear-sky conditions. The GEM UV broadbands are~~ compared to simulated ~~broadbands produced by integrating~~ irradiances generated with Cloud-J, where the ~~high resolution~~ Cloud-J ~~output over~~ calculations were performed using the ~~same spectral regions~~ broadband absorption cross-section and TOA solar fluxes associated to the correlated-$k$ scheme used by GEM for each UV sub-band. ~~Presented are~~ Correlations represent the ~~individual, 7-day~~ single day irradiance ~~contributions from 23-29~~ contribution for 23 August 2015.

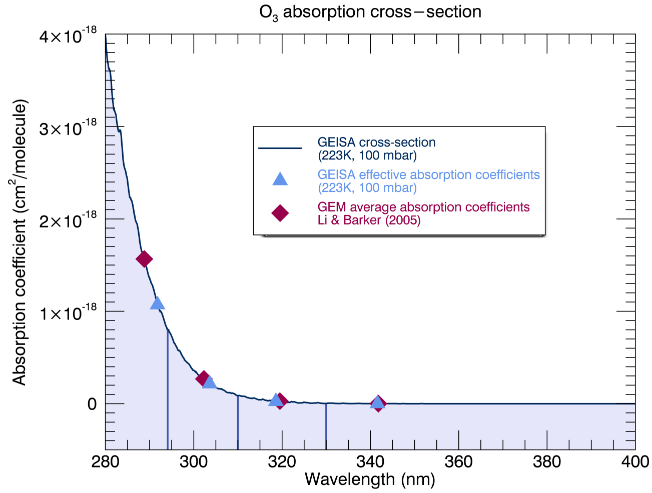


**Figure 7.** ~~GEM broadband surface irradiances compared to simulated irradiances generated with Cloud-J~~ GEISA ozone absorption cross-sections measured at a temperature and pressure of 223 K and 100 mbar, ~~where the Cloud-J calculations were performed using~~ respectively. Overlaid are the ~~broadband~~ effective absorption coefficients calculated from the GEISA cross-section, as described in Sect. 3.1.1, and ~~TOA solar fluxes associated to~~ the ~~correlated-$k$ scheme used by~~ GEM average absorption coefficients for each representative UV ~~sub-band~~ broadband region. ~~Correlations represent the single day irradiance contribution for 23 August 2015.~~

the Brewer measurements and a similar effective resolution of 0.5 nm. For the latter, a boxcar averaging window was applied instead of the ~~trapezoid-shaped~~ approximately triangular-shaped Brewer slit function. Figure 4 depicts 5-day averages of Brewer measurements taken at 18h00 UTC on random days in the months of July and August of 2015 and the equivalent counterpart irradiance spectra calculated from Cloud-J. The locations were chosen to provide *in-situ* measurements for different solar zenith angles in addition to varying geographic locations to evaluate the level of agreement between the Cloud-J model application and the Brewer spectra. Only 5-day averages were used partly due to the limited number of coincident Brewer measurements made during the July-August 2015 period which met the selection criteria for the comparative analysis. Brewer measurements not only had to have been made under clear-sky or near clear-sky conditions, but also were recorded within ∼2 minutes local time of the analogous 18h00 UTC model data.

The Cloud-J derived spectral irradiance curves largely follow those recorded by the Brewers. The differences between the sets of curves give an overall root mean square relative error between the Cloud-J and Brewer spectra of ∼~~15%.~~ 16%. This reflects the level of varying differences over the range of measurement wavenumbers. Some sources that might be contributing to the spectral variability of the differences would include differences between the boxcar averaging for the simulations and an approximately triangular instrument slit function, measurement random errors, and or errors in the TOA spectra for the simulations, if not others. Having large differences visually seen in Fig. 4 to often appear at relative extrema points suggests that the differences of averaging functions may play a notable role in the differences. Investigating this further, including a comparison of applying a triangle-shaped window instead of a boxcar with the simulations, was not done as the overall consistency in spectral shape was considered sufficient for the in this work.

The overall differences in the Cloud-J and Brewer data were also quantified by integrating the spectra of each of the six stations to produce sets of ~~broadbands~~ broadband irradiances covering the 295-310 nm and 310-325 nm regions, the 310 nm node denoting the ~~point transition~~ approximate transition point between the similarly corresponding GEM irradiance broadbands. The resultant mean percent differences of the Cloud-J broadband irradiance values compared to the ground-based measurements for the 295-310 nm and 310-330 nm bands are ~~0.9~~-1.6%±~~4.0% and 7.5~~3.8% and 2.9%±~~1.4~~1.8%, respectively. ~~While not clearly evident from the figure for the lower band, the largest band differences were obtained for Resolute at 5.3% and 9.9%, respectively. Different sources possibly contributing to the variations observed between the model and measurement for each station include :~~ The band mean differences are in the range of uncertainties from the three Brewers inter-comparison by Thompson et al. (1997) and provided above, and within the spread of mean differences in Bais et al. (2001) over the different Brewers and instruments of other types from the SUSPEN inter-comparison for wavelengths above 300-305 nm. Sources affecting the smaller band differences might include disparities in clear-sky to light cloud conditions, surface reflectivities, air pollution, column ozone, and in the actual locations and heights between the Brewer stations and the nearest corresponding model grid points used to represent these locations. Differences in height above sea level between the model grid points and station locations are under 30 m except for Saturna (Fig. 4e) at 26 m versus 202 m and Eureka (Fig. 4c) at 159 m versus 9 m. ~~For example, the lower grid point height for Saturna might be contributing to lower irradiances in the 295-310 nm range relative to most stations when comparing to the Brewer data~~These differences would imply differences in UV Index that are no greater than ∼1.5%, and similar sized differences in the UV irradiances.

Average differences in total column ozone between the GEM model ozone fields provided to Cloud-J simulations and the Brewer measurements for the sample data set of the figure in the range of 2.8 to 4.4% for the four non-Arctic stations and 0.5 and 0.4% for the two Arctic stations of Eureka (Fig. 4c) and Resolute (Fig. 4d). It was determined that the GOME-2 column ozone data used in the assimilation to generate the model forecasts were similarly biased relative to Brewers for that period; satellite data bias can be reduced through corrections such as in van der A et al. (2015). Correcting for the ~~ozone differences~~ larger ozone differences of the non-Arctic stations would increase the Cloud-J irradiances ~~, and thus the differences with Brewers, by at least~~ by 3-5% in the lower band~~for the non-Arctic stations and much less so for the Arctic stations, correspondingly increasing the positive~~ , correspondingly changing differences with the Brewer spectra. The higher band would be less affected as absorption from ozone is comparatively weaker for the upper wavelengths. This would bring the 295-310 nm band irradiance mean differences in percentage closer to the 310-325 nm differences.

~~GEISA ozone absorption cross-sections measured at a temperature and pressure of 223 K and 100 mbar, respectively. Overlaid are the effective absorption coefficients calculated from the GEISA cross-section, as described in Sect. 3.1.1, and the GEM average absorption coefficients for each representative UV broadband.~~ The solar irradiance changes due to the changing orbital earth-sun distance are reflected in the simulations and so would not be a cause of notable differences. The sun itself displays cyclical short-term (solar rotation) and long-term (solar cycle) solar spectrum irradiance variability. In the UV Index spectral range, these changes are within roughly 0.2% and 0.6-1.5% based on measurements over the recent decades (Yeo et al. , 2015; Marchenko et al. , 2016; Mathes et al. , 2017); the total irradiance has a weaker solar cycle change of ∼0.1%. These variations are within the standard deviations of the mean differences over the six stations.

Further analysis of the data sets depicted in Fig. 4 reveal that the ratio of the 310-325 nm to 295-310 nm bands is ~~–~~∼25 for the two Arctic stations and 15 to 17 for the four non-Arctic stations. This illustrates the relative increase of irradiances above versus below ~~310~~ 311 nm for increasing solar zenith angles associated to the stronger increased atmospheric attenuation by ozone in the lower band. As the contribution of the ~~295-310~~ 295-311 nm band to large UV ~~index~~ Index values (low solar zenith angles) is more dominant, the impact of differences above ~~310~~ 311 nm would become more visible on low UV ~~index~~ Index values (high solar zenith angles). Implications of the differing sizes of differences between the ~~295-310nm and~~ ∼295-310 nm and ∼310-330 nm bands and in model ozone forecasts are ~~examined further~~ briefly further examined in Sect. 3.1.3.

~~The source of the usually larger Cloud-J irradiances is not known. This is larger than the 3% uncertainty from the three Brewers inter-comparison by Thompson et al. (1997) but within the spread of mean differences in Bais et al. (2001) over the different Brewers and instruments of other types from the SUSPEN inter-comparison for wavelengths above 300-305 nm. The latter does not however address the overall consistency of the differences of the Cloud-J results over the six Brewers. The solar irradiance changes due to the changing orbital earth-sun distance are reflected in the simulations. The sun itself displays cyclical short-term (solar rotation) and long-term (solar cycle) solar spectrum irradiance variability. In the UV index spectral range, these changes are within roughly 0.2% and 0.6-1.5% based on measurements over the recent decades (Yeo et al. , 2015; Marchenko et al. , 2016; Mathes et al. , 2017); the total irradiance has a weaker solar cycle change of 0.1%. These are too small to account for the differences seen in the 310-325 nm band. Taking the Brewer spectra as reference, the above would suggest a scaling factor adjustment of the Cloud-J irradiances roughly of size 0.93. No such scaling is applied in this paper.~~

### 2.3 Estimation of the UV ~~index~~ Index from GEM broadband irradiances

Two UV ~~index~~ Index estimation approaches using the four broadband irradiances were considered. One consists of linear fitting directly to three of the four UV broadband irradiances, i.e.

$$UVI = w_1 I_{280\text{-}294} + w_2 I_{294\text{-}311} + w_3 I_{311\text{-}330} + w_4 I_{330\text{-}400} \quad (3)$$

with $I_{\Delta\lambda}$ in W/m$^2$ and fit coefficients $w_i$. With this equation, the contribution from the lowest band can be neglected unless the total column ozone is less than roughly 210 DU to contribute at least 0.1 units to the UV ~~index~~Index. Its coefficient value $w_1$ is analytically derived to be 40 m$^2$/W since the erythemal action spectrum is constant over the spectral range of the lowest band.

The other approach involves applying the integral of Eq. (2) to piecewise interpolated spectra. Both fits are intended to have the UV ~~index~~ Index values derived from the broadband irradiances be consistent with the values obtained from the integrated high resolution effective spectra. UV ~~index~~ Index values larger than 3 are used in the minimization to focus the weighting on regions of moderate to high UV ~~index~~ Index values. The fitting over points with UV ~~index~~ Index values larger than 3 does not exclude points and regions with isolated outlier differences and includes both land, water, and snow/ice surfaces. Minimization was performed using an amoeba downhill simplex method employing a least-squares fitting of the UV ~~index~~ Index fields from the scaled GEM broadband irradiances to those from the high resolution spectra produced by Cloud-J.

For the integral approach, the available irradiances in W/m$^2$ over the four UV spectral broadbands must be transformed to spectral irradiances for multiplication to the erythemal function prior to spectral integration. The approximate conversion to spectral irradiances is done as follows:

1. The band irradiances are divided by the band widths to generate average spectral irradiances.

2. Each of the resulting average spectral irradiances in W/(m$^2$/nm) is associated with a particular reference spectral position to be determined through fitting.

3. Logarithmic first or second order Lagrange interpolation is applied over each piecewise spectral integration interval without forcing agreement at the band interfaces.

The selected order of the logarithmic interpolations and initial estimates of the spectral reference positions were chosen through trial and error. The optimized spectral positions are determined through least-squares fitting to the UV ~~index~~ Index values calculated from the Cloud-J high spectral resolution irradiances.

Interpolations and weighted integrations are performed over four segments covering the ranges 294-298, ~~298-310, 310-328~~ 298-311, 311-328, and 328-400 nm. The irradiance for 280-294 nm is simply added to the sum of the integrations over the above four ranges as the erythemal function is constant with a value of unity over that spectral range; its contribution over this integration segment could alternatively be omitted as it is negligible. Determination of a reference spectral irradiance for this first band in step 2 above is still done to provide a required interpolation node for the other integration segments. The specification of the segments is dictated by the band widths and the two positions, 298 nm and 328 nm, of the slope changes in the erythemal function.

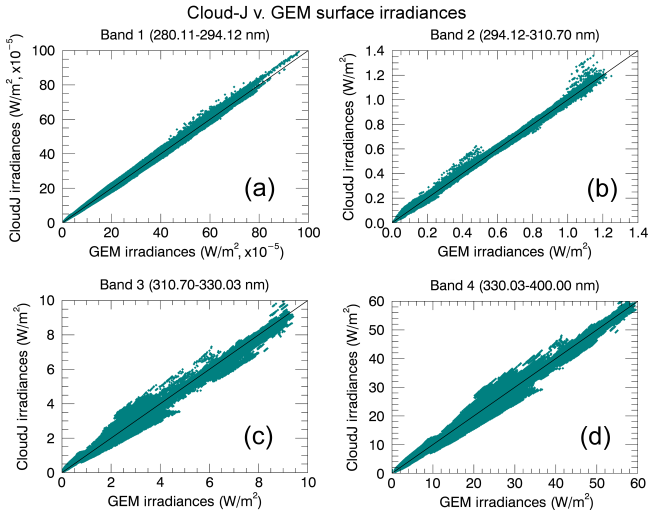


**Figure 8.** Calibrated GEM broadband irradiances, corrected using the total irradiance scaling functions found in Table 1, compared to the simulated GEM broadband irradiances produced by Cloud-J.

The applied interpolations are of second order for the ranges 294-298 and ~~310-328~~ 311-328 nm and are linear in the other ranges. The simple interpolations do not strictly preserve the original broadband irradiance values nor accurately replicate high resolution spectra since the main interest is the fast computation of good estimates of the resultant integral value. The integrations for the last three segments are done using Simpson~~?~~'s rule with two subintervals (5 interpolation nodes) and that for 294-298 nm is done with one interval (3 interpolation nodes).

## 3 Results

### 3.1 Clear-sky conditions

#### 3.1.1 Broadband irradiances

The comparisons made between GEM and Cloud-J broadband irradiances for clear-sky conditions shows a fairly good agreement in the ~~310-330~~ 311-330 nm and 330-400 nm bands. For these bands, the linear correlation agreement between the two models is typically greater than 95% with associated root mean square relative errors of ~~5.5% and 3.8~~6.4% and 4.0% for midday values. On the other hand, underestimations of GEM irradiances were found in the order of ∼30-50% for ~~294-310~~ 294-311 nm band and by a factor of ∼30 for the 280-294 nm band as shown in Fig. 5b and Fig. 5a, respectively. It was subsequently identified that the bulk of the differences for the two lower bands, especially the disparity in curvatures in bands 1 and 2 of Fig. 5, stems from differences in equivalent broadband absorption cross-sections if not also TOA solar fluxes. This is further supported by the significantly improved agreement demonstrated in Fig. 6 where the cross-sections of the correlated-*k* approach cited in Table 6 of Li and Barker (2005) and the solar broadband top of the atmosphere (TOA) fluxes employed by the GEM model were instead applied in the Cloud-J calculations. It should be noted that the band solar fluxes used in GEM differ by approximately 0.02% to 0.15% from the UV sub-band solar fluxes reported in Table 6 of Li and Barker (2005).

A direct comparison was made between the GEM TOA solar fluxes and the broadband averages that were calculated from Cloud-J using the data obtained from Dobber et al. (2008). There are significant differences in the two short-wavelength broadbands with the band values calculated from the Dobber et al. (2008) fluxes being smaller than the GEM fluxes by 35% and 15% for the 280-294 and ~~294-310~~ 294-311 nm bands, respectively; values for the higher bands are only 3% smaller and 2% larger, respectively. These differences would favour an underestimation of the Cloud-J irradiances relative to GEM at the shorter wavelengths in the absence of differences in cross-sections, which is opposite to the results in Fig. 5. A comparison to the band averages derived from the solar flux spectrum of Chance and Kurucz (2010) gives smaller differences of -12%, 2%, -1% and 3.5% relative the GEM values.

~~Calibrated GEM broadbands, corrected using the total irradiance scaling functions found in Table 1, compared to the simulated GEM broadbands produced by Cloud-J.~~

The spectrally, uniformly-weighted average cross-sections from the GEISA dataset which represent the four UV ~~broadbands~~ broadband irradiances are about 24-32% larger than the values reported in Table 6 of Li and Barker (2005), this also being inconsistent in implication with Fig. 5. However, these estimates do not account for the non-linear impact of the strong spectral variation of absorption cross-sections from the GEISA database at lower wavelengths in the UV spectral range shown in Fig. 7. Effective band cross-sections from the GEISA spectrum were also calculated for each spectral region for irradiances at the surface using

$$c_{eff} = \frac{1}{N} \cdot \ln\left[\frac{\sum F_\lambda \Delta\lambda}{\sum F_\lambda \mathrm{e}^{-Nc_\lambda} \Delta\lambda}\right] \tag{4}$$

where $F_\lambda$ denotes the solar spectral irradiances in W/(m$^2\cdot$nm), $c_\lambda$ are the absorption coefficients set for a reference temperature and pressure of 223 K and 100 mbar, and the $N$ is a total column ozone of 8.07x10$^{18}$ molecules/cm$^2$, equivalent to 300 DU. The numerator is equivalent to deriving broadband average solar fluxes from equally weighting values over all wavelengths as in the previous paragraph. The effective cross-section estimates calculated from Cloud-J for the two lowest UV bands (280-294 nm and ~~294-310~~ 294-311 nm), with values of 1.09x10$^{-18}$ and 2.20x10$^{-19}$ cm$^2$/molecule respectively, are now instead smaller by 31% and 19% relative to the cross-sections referred in Li and Barker (2005) implying larger Cloud-J irradiances; values are larger for the higher wavelength bands by 5% (313-330 nm) and 18% (330-400 nm). The impact of these differences is made stronger for the lower bands as their absorption cross-sections are larger than for the higher bands by an order of magnitude or more; absorption by ozone in the higher bands is comparatively much weaker. The implied tendency is now in agreement with Fig. 5. This suggests weaker atmospheric attenuation at least from using the GEISA cross-section dataset instead of the broadband absorption cross-sections associated to the correlated-*k* approach. Taking the spectrally dependent cross-sections and solar fluxes used with Cloud-J as more reliable references, then one or both elements of the broadband cross-section and solar flux pairs associated to Li and Barker (2005) and GEM for the lower bands could be considered less optimal for determining irradiances at the surface. This stance is supported by the better agreement, for non-polar stations in Sect. 2.2, between the Cloud-J and Brewer sample spectra especially for the dominant ~~295-310~~ 295-311 nm band.

Considering the above analysis of the differences in broadband irradiances shown in Fig. 5, scaling of the GEM irradiances to the Cloud-J broadband irradiances was applied

**Table 1.** Sets of scaling functions to calibrate the GEM UV ~~broadbands~~ broadband irradiances to emulate the simulated ~~broadbands~~ broadband irradiances produced by Cloud-J. Functions were obtained for total surface irradiances and also their direct and diffuse components.

| Wavelength range | GEM UV broadband irradiance scaling functions<br>Total irradiance (W/m$^2$) | Direct component (W/m$^2$) | Diffuse component (W/m$^2$) |
|---|---|---|---|
| ~~280-294~~ 280.11-294.12 nm | | 310.70-330.03 nm | 294.12-310.70 nm<br>$\cancel{f(x) = 0.973x}$ $f(x) = 0.953x$ |
| $\cancel{f(x) = 1.048x}$ $f(x) = 1.026x$ | $\cancel{f(x) = x^{0.892}}$ $f(x) = x^{0.872}$ | | |
| ~~330-400~~ 330.03-400.00 nm | $\cancel{f(x) = 0.993x}$ $f(x) = 0.985x$ | $\cancel{f(x) = 1.031x}$ $f(x) = 1.025x$ | $\cancel{f(x) = x^{0.970}}$ $f(x) = x^{0.965}$ |

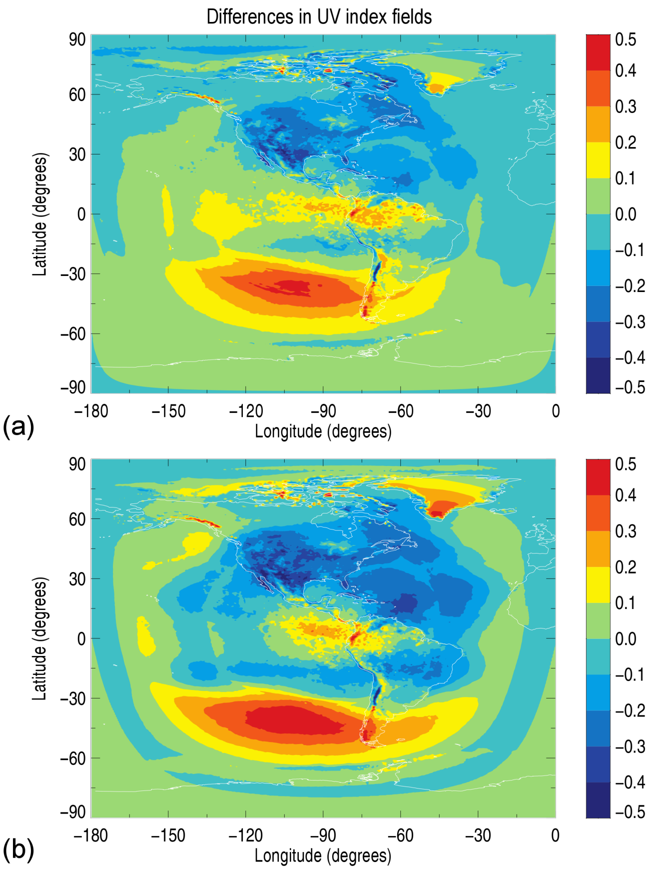


**Figure 9.** Differences in the UV Index field produced from the scaled and weighted GEM irradiances compared to the field produced using the high resolution Cloud-J irradiances for the integration approach and linear fit, representing plots (a) and (b) respectively.

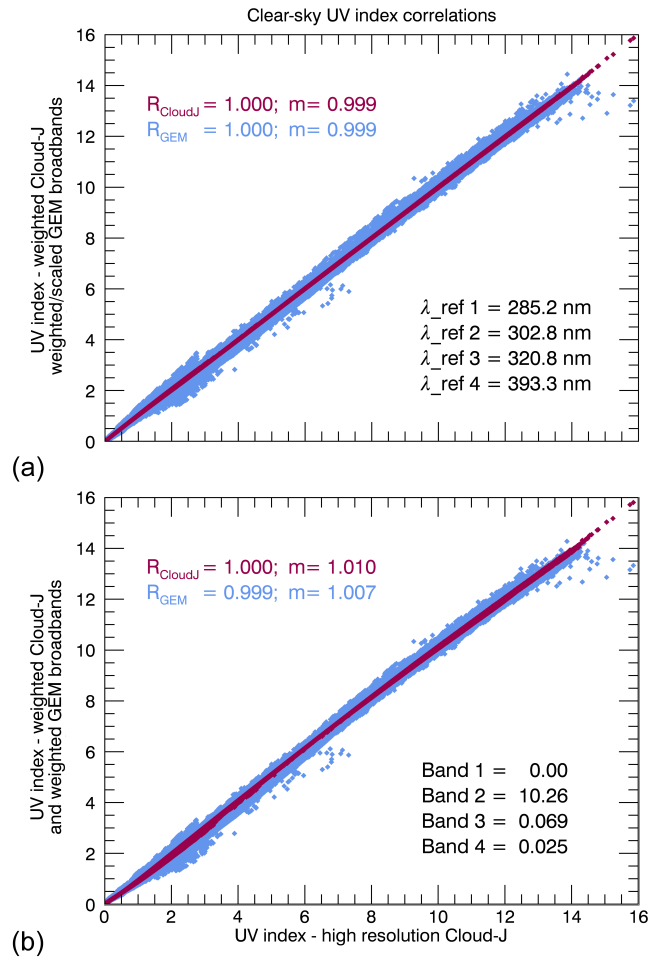


**Figure 10.** Correlation of the UV Index fields generated from the Cloud-J (purple) and GEM (blue) broadband irradiances. Results from the least-squares minimization using the integration approach (upper panel, a) produced reference positions of 285.2, 302.8, 320.8, and 393.3, respectively for each UV sub-bands. Minimization performed using the direct linear fitting method (lower panel,b) produced coefficients of 10.26, 0.069, and 0.025 for bands 2 through 4, respectively, where the weighting for band 1 was intentionally fixed to a value of zero.

as functions of the irradiance values for each spectral band. While contributions to the UV ~~index~~ Index from the 280-294 nm band itself could be neglected for total column ozone above roughly 150 DU, scaling functions for this band were still generated since the band value is used in the spectral interpolation to higher wavenumbers for the second UV ~~index~~ Index model of Sect. 3.1. Also, scaling for the two highest UV bands is not essential and was done here for completeness. Fits were generated using the 7-day contributions for the total, direct, and diffuse irradiances of the four bands under clear-sky conditions (23-29 August 2015). The scaling functions are provided in Table 1. The correlation of the broadband Cloud-J and the scaled GEM total irradiances obtained for clear-sky conditions are provided in Fig. 8.

#### 3.1.2 UV ~~index~~ Index from broadband irradiances

The UV ~~index~~ Index fitting based on the Sect. 2.3 integral approach applied to GEM scaled broadband irradiances provided reference positions of ~~285.3, 302.7, 320.3, and 379.4~~ 285.2, 302.8, 320.8, and 393.3 nm for bands 1 through 4, respectively, while the straight forward linear fit yielded:

$$UVI = \cancel{11.03}10.26 I_{\cancel{294\text{-}310}294\text{-}311} + \cancel{0.084}0.069 I_{\cancel{310\text{-}330}311\text{-}330} + \cancel{0.0290} \qquad (5)$$

~~Differences in the UV index field produced from the scaled and weighted GEM irradiances compared to the field produced using the high resolution Cloud-J irradiances for the integration approach and linear fit, representing plots (a) and (b) respectively.~~

where the first coefficient was derived analytically as mentioned in Sect. 2.3. Most of the sensitivity to ozone variability is typically reflected in $\cancel{I_{294-310}}$ $I_{294-311}$ as absorption from ozone is comparatively weaker for the upper wavelength bands. Reductions in column ozone by 20% from 300 DU imply changes of about 38%, 8.6%, and 0.15% in UV ~~index~~ Index from the last three terms, respectively, when the sun is directly overhead.

~~Correlation of the UV index fields generated from the Cloud-J (purple) and GEM (blue) broadbands. Results from the least-squares minimization using the integration approach (upper panel, a) produced reference positions of 285.3, 302.7, 320.3 and 379.4, respectively for each UV sub-bands. Minimization performed using the direct linear fitting method (lower panel,b) produced coefficients of 11.03, 0.084, and 0.029 for bands 2 through 4, respectively, where the weighting for band 1 was intentionally fixed to a value of zero.~~

Differences of the clear-sky UV ~~index~~ Index field between the Cloud-J and resulting GEM values are shown in Fig. 9 and are found to be typically less than 0.2-0.3 for both the integration (upper panel, a) and linear fit (lower panel, b) approaches. The integration approach provides better agreement to Cloud-J, this by up to about 0.1-0.2 for some locations. Over North America, the resultant UV ~~index~~ Index values are usually smaller than the Cloud-J based values by 0.1 to 0.3. Both plots also demonstrate an extended circular region at high zenith angles in the Southern Hemisphere with positive differences reaching up to ~~-~~ ∼0.5 in the South Pacific area. These larger differences are coincident with UV ~~index~~ Index values near the threshold value of 3 used in the least-squares minimization of the scaled GEM ~~broadbands~~ broadband irradiances to the high resolution UV ~~index~~ Index field produced by Cloud-J. In addition, there are a sparse number of hot spots which are primarily confined to the Arctic and the high altitude regions of the Western Cordilleras of North and South America. Here, the differences in the UV ~~index~~ Index range between 0.2 to an extreme of 2.4, where the largest differences are confined to a few isolated mountain peaks in Ecuador and the Southern Patagonian Ice Fields bordering Argentina and Chile. The source of the hot spots were determined to be originating from the diffuse component of the calculated surface irradiances, where it was ascertained that the cause was ultimately due to differences in the albedo values used by the GEM and Cloud-J models, where the GEM albedo values underestimate the snow/ice reflectivities in these regions. UV surface reflectivities for snow/ice are typically >85% (Chadyšien and Girgždys , 2008), and are readily observed in the OMI monthly average surface reflectivities used by Cloud-J. Although the GEM albedo values for these same regions are also elevated, with respect to the surrounding terrain, they are typically smaller as compared to the OMI-based climatology by 35-50%.

Curiously, there exists a notable cold spot in the plots of Fig. 9, and it too occurs in South America along a large barren desert tract of the Andes mountains in northwestern Argentina, northern Chile, and southwestern Bolivia. Here, the

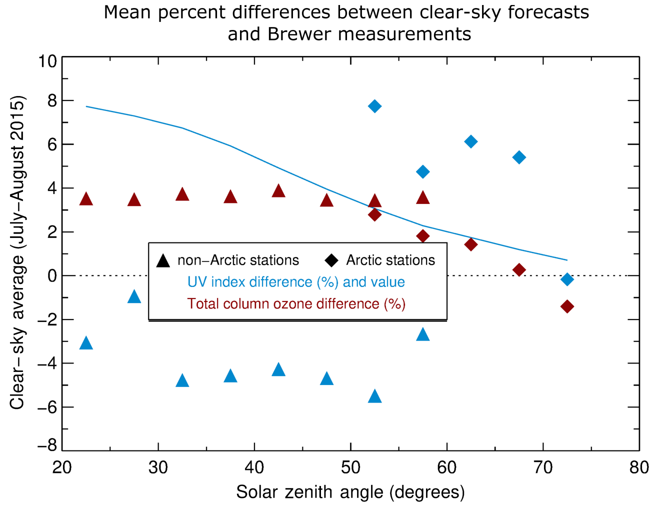


**Figure 11.** Average UV ~~index~~ Index and total column ozone relative differences between the model forecasts and Brewer measurements as a function of solar zenith angle for daytime clear-sky to lightly cloudy conditions for both sets over July and August 2015. This is accompanied by the corresponding average UV ~~index~~ Index values. The averages are over 5 degree intervals in solar zenith angles over the two Arctic stations (Eureka and Resolute) and four non-Arctic stations (Churchill, Edmonton, Saturna and Toronto) of Fig. 4. The resultant numbers of averaging points per bin range from 30 to 1002 with statistical outliers having been removed in final averages. Model ~~short-term~~ forecasts with output for station locations every ~~12~~ 7.5 minutes were generated from weather and ozone analyses ~~at~~ for 00 ~~, 06, 12,~~ and ~~18~~ 12 UTC.

GEM model indicates that surface reflectivities are elevated to values ranging from 60-75%, much higher than those associated with the snow/ice albedos representing the Southern Patagonian Ice Fields. OMI, on the other hand, produces reflectivities of only 10-15%, making little distinction with the surrounding landscape. Further investigation reveals that this region is variably snow-covered during the winter months of the Southern Hemisphere, where the presence of snow is not consistent throughout the month or from year-to-year. During the 23-29 August 2015 analysis period used our study, this corresponding region of the Andes was covered under a fresh layer of snow. This observation is corroborated by both snow depth (SD) data obtained from the GEM model, and through visual confirmation using imagery data provided by the Moderate-Resolution Imaging Spectroradiometer (MODIS) instruments onboard the Aqua and Terra satellites (https://worldview.earthdata.nasa.gov/). Since the OMI albedo data represents monthly mean reflectivities over a 5 year period (2005-2009), it is unsurprising that a variable presence of snow in this region creates disparities with the long-term averaged values recorded by OMI. The averaging would result in an underestimation in the OMI reflectivites, thus creating the observed cold spot seen in Fig. 9(a and b).

Figure 10 shows the resultant direct correlations between clear-sky UV ~~index~~ Index values obtained from the high resolution effective spectra versus those from the broadband Cloud-J and GEM irradiances for both the integration approach (a) and direct linear fit (b) for the data corresponding to the 7-day contributions over North America and the Arctic on August 23-29, 2015, at 18 UTC. The integration approach, used to weight the scaled GEM ~~broadbands~~ broadband irradiances (cyan), show an excellent agreement with the UV ~~index~~ Index calculated using the Cloud-J ~~broadbands~~ broadband irradiances (purple) where the slope of the curves, m, and associated Pearson correlation coefficients, R, are at unity. The resultant differences in UV indices from the high spectral resolution irradiances and the resultant GEM broadband irradiances are typically within 0.2 with a root mean square relative error in the scatter of ∼~~5.3~~5.6% for clear-sky conditions. The UV indices calculated using the direct linear combination fitting of the GEM ~~broadbands~~ broadband irradiances produce similar results with a root mean square relative error in the scatter of ∼~~6.6~~7.8% for UV ~~index~~ Index values larger 3.

### 3.1.3 Comparison to ground-based UV ~~index~~ Index measurements

Section 2.2 provided a comparison of simulated Cloud-J and measured Brewer sample irradiance spectra. The comparison with Brewer measurements is extended here to the clear-sky UV ~~index~~ Index and column ozone values from the GEM model ~~short-term~~ 24-hour forecast output at 7.5 minute intervals over successive twelve hour forecasts covering July and August of 2015. Figure 11 shows average differences in total column ozone between ~~model short-term forecasts~~ the model output and Brewer measurements in the range of 3.5~~to 3.9~~-3.9% for the four non-Arctic stations with a decrease toward zero at higher latitudes for the two Arctic stations, Eureka and Resolute. This is consistent with column ozone differences stated in Sect. 2.2.

~~The UV index average values corresponding to the column ozone values~~ Values for the average UV Index corresponding to their associated column ozone concentrations were generated from the model ~~short-term forecasts~~ output using the simplified spectral integration approach. The average UV ~~index~~ Index differences between the model forecasts and the Brewers are ~~-2.5 to -5~~-1 to -6% for the non-Arctic stations, which is partly explained by the differences in column ozone, ~~to 6-9~~and 0-8% for the two Arctic stations. ~~The larger percentages~~

The typically larger percentage values for the two Arctic stations ~~partly reflect relative increase~~ might be partly attributed to the relative increases in contribution from irradiances for bands above versus below ~~310~~ 311 nm at higher solar zenith angles combined with the ~~larger~~ mean irradiance differences with Brewers above ~~310 nm~~and below 311 nm, mentioned in Sect. 2.2. ~~This difference is not inconsistent with the 7.5% overestimation of the Cloud-J 310-325 nm band irradiance indicated in that same section and for which no scaling currently has been applied. The source of differences of the UV index comparisons~~The cause of the high-latitude disparity in the UV Index observed when comparing between the non-Arctic and Arctic stations in the overlap 50-60 degree region of Fig. 11 is not known. One possibility may be linked to a geographically varying residual error of the GEM UV Index relative to the Cloud-J value. Still, considering the small UV ~~index~~ Index values at high solar zenith angle larger than ~~∼~~∼50 degrees, these translate to absolute differences with Brewers of less than 0.4.

The negative differences in UV ~~index of -2.5 to -5~~Index of -1 to -6% for the non-Arctic stations ~~differ from the overall slightly positive~~ are usually larger (towards the negative) than the differences of Cloud-J irradiances from Fig. 4~~based on the five cases at 18 UTC for each station~~. Potential contributing sources of these differences are the residual errors from the fits for irradiances and for the UV ~~index~~Index, the latter having been performed considering only for values larger than 3; Fig. 9 indicates roughly -0.1 to -0.3 differences between GEM and Cloud-J over much of Canada. Reducing model ozone biases would improve the agreement with clear-sky Brewer UV ~~index~~ Index values by a few percent for UV ~~index values above~~ Index values above ∼3-4 ~~and~~ or solar zenith angles below 50-60 degrees. ~~Additionally incorporating the 0.93 scaling factor correction alluded to in Sect. 2.2 would bring these differences back to about -5 to -7%, or roughly -0.3 to -0.5, while improving results for the Arctic Stations.~~

## 3.2 Cloudy-sky conditions

As described in Sect. 1.2, the Cloud-J model possesses a number of options for the treatment of clouds in its radiative transfer calculations. Cloud-J ~~broadbands~~ broadband irradiances were produced for each of the cloud options representing cloudy-sky conditions, 2-8, using the GEM parameters for liquid and ice water partial column amounts of each model layer in the presence of clouds and the associated cloud fractions, which are required input for Cloud-J. The simulated ~~broadbands~~ broadband irradiances produced by Cloud-J for each cloud option were then compared to the GEM analogs to determine which Cloud-J cloud flag produces output that best reproduces the GEM cloud-sky surface irradiances.

Prior to performing the comparative study, it was recognized that fundamental differences existed between Cloud-J and GEM with respect to the handling of clouds, particularly with respect to the scattering of light with parameters specific to water droplet/ice crystal size. Unlike GEM, the Cloud-J model does not specifically differentiate water droplets and ice crystals into different size bins and determine the scattering contribution accordingly. Instead, for water, an average droplet size is determined for the total water content in

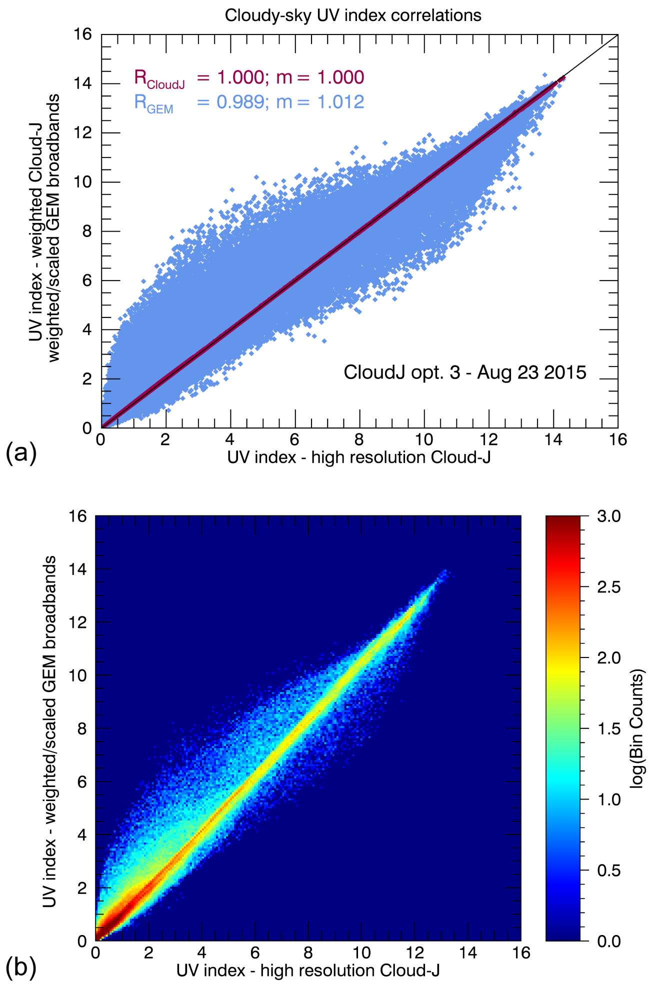


**Figure 12.** Analogous correlations of the UV ~~index~~ Index fields generated from the Cloud-J (purple) and GEM (blue) ~~broadbands~~ broadband irradiances under cloudy-sky conditions using Cloud-J cloud flag Option 3 in the comparison. The upper panel, a, presents the direct linear correlations of the UV ~~index~~ Index calculated using the GEM and Cloud-J ~~broadbands~~ broadband irradiances relative to the high resolution output produced by Cloud-J using the same scaling functions and weighting determined through the integration approach under clear-sky conditions. The lower panel, b, is a density plot of the correlation of the UV ~~index~~ Index calculated using the GEM ~~broadbands~~ broadband irradiances compared to the Cloud-J, high resolution, UV ~~index~~ Index field depicted in the upper panel.

a particular model layer depending on the temperature and pressure associated with the model layer. Ice crystals are not differentiated by size at all, only by crystal shape (hexagonal, amorphous), which is also determined by the given temperature and pressure of the model layer. Ultimately, it was determined that Cloud-J cloud option 3 produced cloudy-sky surface irradiances that best emulated the GEM analog. This option was therefore applied for the UV ~~index~~ Index comparisons in this section.

The estimation and evaluation of the UV ~~index~~ Index estimated under cloudy conditions in this study has been limited to the consideration of two points. One is whether or not the UV ~~index~~ Index equations derived from clear-sky conditions are appropriate for cloudy conditions. The other is determining the level of impact of radiative transfer differences in the treatment of clouds on differences in derived UV ~~index~~ Index values.

The validity of the clear-sky UV ~~index~~ Index equations for cloudy conditions was tested using Cloud-J simulations. The clear-sky equations were applied to the Cloud-J broadband irradiances for comparison to the UV ~~index~~ Index values derived from the high resolution Cloud-J spectra for the actual sky conditions from GEM-LINOZ, the latter being a mixture of clear-sky and cloudy-sky conditions. It was found that the equations derived for clear-sky conditions and applied to cloudy conditions with Cloud-J ~~broadbands~~ broadband irradiances give essentially the same results as the UV ~~index~~ Index values from the high resolution spectra, i.e., no visible scatter about the diagonal is observed for the corresponding differences in Fig. 12a. Therefore, these equations would also be valid under cloudy conditions and do not require further adjustment.

The remainder of this section examines the impact of differences in cloud radiative transfer. Figure 12a shows the analogous correlations of the UV ~~index~~ Index fields generated from the Cloud-J and GEM ~~broadbands under all sky~~ broadband irradiances under all-sky conditions using the Cloud-J cloud option 3. The weighting was performed using the values obtained though the integration approach of the GEM ~~broadbands~~ broadband irradiances under clear skies. Weighting of the ~~all sky broadbands~~ all-sky broadband irradiances using the values obtained from the linear fitting approach produce similar results. The overall correlation of the Cloud-J data is in fairly good agreement with the GEM data, but there is an overall increase in error between the two data sets with increasing values of the cloud fraction. To better visualize the distribution density of the correlation, a density plot is also provided in Fig. 12b. We observe that the vast majority of points fall along or near the regression line, ~~and ultimately~~ largely, but not entirely, represent those surface irradiances under cloudless ~~, clear-sky~~or light-cloud, conditions. ~~Deviation~~ The probability of deviation from the regression line typically increases with increasing cloud cover. ~~Overall, the resultant differences in UV indices from the high spectral resolution irradiances and the resultant GEM broadband irradiances are similar under cloudy conditions with light to moderate clouds, having a relative error comparable to the clear-sky counterpart, but under strong attenuation due to clouds, a substantial increase in the root mean square relative error of up to 33% is observed due to differing cloud radiative transfer models for UV index values of 1 or larger~~This is demonstrated below with Fig. 13.

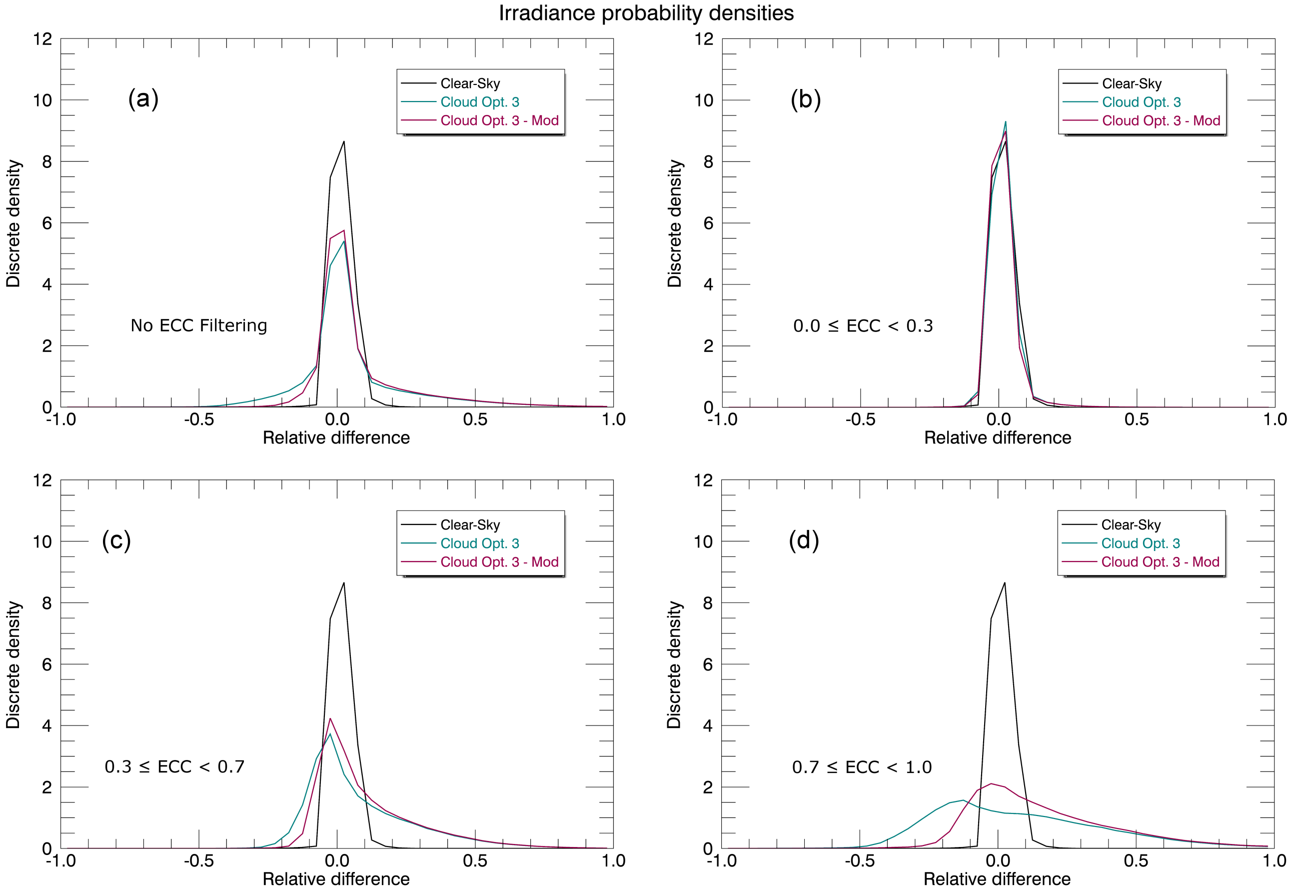


**Figure 13.** Irradiance probability density plots demonstrating the dependence of the 330-400 nm surface irradiances on effective cloud cover (ECC). Plotted are the relative differences between the Cloud-J and GEM surface irradiances under unattenuated, clear-sky conditions (black), cloudy-sky where the Cloud-J Option 3 cloud flag is used to calculate cloud attenuation (green), and a modified version of the GEM model output for cloudy skies compared to the Cloud-J data employing the Option 3 cloud flag (purple). The modification made to the GEM code was to change the effective radii for the ice clouds to determine if it made any difference relative to the Cloud-J output. In all four plots, a solar zenith angle filter was applied, where only surface irradiances pertaining to locations where zenith angles <70°are used. A secondary filter for varying total effective cloud cover is employed in the plots to display the relative difference in irradiances for a given range of cloud cover from clear-sky (0.0) to completely overcast (1.0).

Figure 13 contains a series of probability density plots to visualize the dependence of differences in surface irradiances on cloud cover for the 330-400 nm band. Relative differences are observed between the Cloud-J and GEM surface irradiances under unattenuated, clear-sky conditions, as well as for different total effective cloud fraction intervals. To filter for cloud cover, we used the GEM variable for total effective cloud cover (ECC) ~~was used~~which reflects the product the the cloud fraction and opaqueness. ECC is employed in the plots to display the relative differences of the GEM and the Cloud-J irradiance values for a given range of cloud cover from clear-sky (0.0) to completely overcast (1.0). Only surface irradiances pertaining to zenith angles < 70°were included to remove larger systematic relative differences at high zenith angles where irradiance values are smaller. The Cloud-J cloud option 3 is used to calculate cloud attenuation in all cases. Output from two different settings of the GEM radiative transfer package for cloudy skies are separately provided for Cloud-J simulations and compared to the corresponding GEM irradiances.

Overall, the resultant differences in UV Index values from the high spectral resolution irradiances and the GEM broadband irradiances have a similar distribution for ECC < 0.3 as that for clear-sky conditions (Fig. 13b). Under stronger attenuation due to clouds, a substantial increase in the root mean square relative error of up to 33% is observed due to differing cloud radiative transfer models, this involving UV Index values of 1 or larger.

The modification made to the GEM code from its reference settings of Sect. 1.1 was to increase the overall size of the effective radii for the ice clouds from a constant of 15 $\mu$m to values in the range of 20-50 $\mu$m to determine if it made any difference in relation to the Cloud-J output. As noted earlier in this section, Cloud-J does not differentiate between particle sizes in ice clouds. In the plots, we observe the increase range of relative differences with increasing cloud cover where differences can reach as high as 100% and above where the cloud fraction is $\geq 0.7$ (Fig. 13d). This implies, that different cloud radiative transfer settings ~~or models~~(and models) can result in very large differences in UV ~~index~~ Index in the presence of optically thick clouds. Also notable, is the overall improvement on the left-hand side of the distributions when the ice particle size was increased. This illustrates the sensitivity of irradiances to cloud related model parameters. To quantify this sensitivity, the percentage contribution of the total discrete densities are compared for the relative differences in the ranges of -0.2 to 0.2 for cases representing $0.3 \leq$ ECC $< 0.7$ (moderate to heavy cloud) and ECC $\geq 0.7$ (heavy cloud to completely overcast) conditions, (Fig. 13c) and (Fig. 13d), respectively. Under moderate ~~cloud~~ to heavy cloud cover, the density distributions are similar in nature, where the percent contributions for both the modified and unmodified versions of the GEM model are $\sim$~~77~~76%. For heavy cloud to completely overcast skies, there is a marked difference in the percent contributions. The unmodified GEM model cloud scheme produces a distribution where 50% of the discrete density is located within the -0.2 to 0.2 range for the absolute relative differences. Using the modified scheme, this value is increased to 62% stemming from more relative differences of smaller absolute size. These results and percentages provide some general sense of the potential uncertainties of the UV ~~index~~ Index values given possible uncertainties in the accuracy of the cloud radiative transfer models.

## 4 Conclusions

A successful optimization of UV ~~index~~ Index determination from broadband irradiances was performed. The Cloud-J v7.4 radiative transfer model was adapted to provide high spectral resolution surface irradiances in the UV, 280-400 nm. The high resolution output from Cloud-J is used to evaluate ECCC's GEM forecast model broadband irradiances under clear-sky conditions and to optimize the determination of the UV ~~index~~ Index using these coarse ~~resolution spectral~~ spectral resolution irradiance broadbands.

The optimization is achieved by creating simulated ~~broadbands~~ broadband irradiances using Cloud-J for direct comparison with the GEM broadband irradiances to generate sets of scaling functions to calibrate the GEM values to the Cloud-J output. The scaled GEM ~~broadbands~~ broadband irradiances are weighted accordingly such that the global UV ~~index~~ Index field produced using the coarse resolution ~~broadbands~~ broadband irradiances subsequently replicate the high resolution UV ~~index~~ Index field calculated from Cloud-J. Further optimization with the current setup could still be performed, such as excluding outlier differences and focusing over land areas in the fits, and further exploring the differences with the Brewer UV irradiance spectra and UV ~~index~~ Index values. The comparison with Brewer data for clear-sky conditions suggests potentially remaining systematic UV ~~index~~ Index differences up to about 0.3 to 0.5 in magnitude when the surface reflectivities are sufficiently representative.

It was established that equations for the UV ~~index~~ Index calculation determined from clear-sky conditions are also applicable to cloudy conditions. However, as is to be expected, the quality of the UV ~~index~~ Index values strongly depend on the accuracy of the representation of clouds and, as implied in the limited evaluation of Sect. 3.2, on the accuracy of the cloud radiative transfer model. With formulations as developed here, the improvement of the quality of the UV ~~index~~ Index would follow the improvement in accuracy of these factors.

Outlier differences in UV ~~index~~ Index values under clear-sky conditions exemplified the relevance of using sufficiently representative surface reflectivities for snow and ice covered surfaces. Other factors, such as changes in the applied aerosol climatology or adjustments in the clear-sky irradiance calculation model might potentially warrant a revisiting of the fit coefficients.

The model simulations from Cloud-J, GEM, and similarly from other numerical prediction models, pertain only to the consideration of atmospheric columns directly overhead. While the solar zenith angle is reflected in the overhead column attenuation, the atmospheric conditions along the slanted viewing column may differ thus affecting the actual surface irradiances and UV ~~index~~Index. Moreover, for non-uniform cloud opacity, cloud scattering from various directions is unlikely to be correctly reflected from the overhead column or the solar viewing column alone. Accounting for these aspects, which is beyond the scope of this study, could further improve the accuracy of UV ~~index~~ Index forecasts.

*Code and data availability.* The availability of the Cloud-J v7.4 radiative transfer model, and the various data sets used in the model modifications to calculate high-resolution surface irradiances including the TOA solar spectrum, $O_3$ cross-sections, surface reflectivities, and Rayleigh scattering parameters are detailed in Sect. 2 of this publication. The output for the GEM forecast data and GEM-LINOZ $O_3$ fields are saved with an in-house binary file format; this in-house, binary file format is used to store gridded data from numerical weather and chemical prediction models, objective analyses and geophysical fields. Code changes made to Cloud-J to make use of such files takes advantage of in-house libraries. Selected data from these files, which can be reproduced in other desired formats, and related diagnostic results can be made available upon request.

*Competing interests.* The authors declare that they have no conflict of interest.

*Acknowledgements.* The authors would like to thank the Natural Sciences and Engineering Research Council of Canada (NSERC) for supporting K. A. Tereszchuk through the Visiting Fellowships in Canadian Government Laboratories Program (Grant: 462244-2014)), Michael Prather of the University of California, Irvine, for information on usage of Cloud-J, Quintus Kleipool of the Royal Netherlands Meteorological Institute for providing the solar spectrum, Vitali Fioletov and Akira Ogyu from ECCC regarding information on Brewer measurements, Jean de Grandpré and Irena Ivanova (ECCC) for assistance in use of the GEM-LINOZ model, and Louis Garand (ECCC) for suggesting use of the GEM broadband irradiances for UV ~~index~~ Index determination.

## References

Allaart, M., van Weele, M., Fortuin, P. and Kelder, H.: An empirical model to predict the UV-index based on solar zenith angles and total ozone, Meteorol. Appl., 11, 59–64, doi:10.1017/S1350482703001130, 2004.

Bais, A. F., Gardiner, B. G., Slaper, H., Blumthaler, M., Bernhard. G., McKenzie, R., Webb, A. R., Seckmeyer, G., Kjeldstad, B., Koskela, T., Kirsch, P. J., Grobner, J., Kerr, J. B., Kazadzis, S., Leszczynski, K., Wardle, D., Josefsson, W., Brogniez, C., Gillotay, D., Reinen, H., Weihs, P., Svenoe, T., Eriksen, P., Kuik,F., and Redondas, A.: SUSPEN intercomparison of ultraviolet spectroradiometers, J. Geophys. Res., 106, 12509-12525, 2001.

Bian, H. and Prather, M. J.: Fast-J2: Accurate Simulation of Stratospheric Photolysis in Global Chemical Models, J. Atmos. Chem., 41, 281–296, doi:10.1023/A:1014980619462, 2002.

Burrows, W. R., Vallée, M., Wardle, D. I., Kerr, J. B., Wilson, L. J., and Tarasick, D. W.: The Canadian operational procedure for forecasting total ozone and UV radiation, Met. Apps., 1, 247–265, doi:10.1002/met.5060010307, 1994.

Burrows, J. P., Richter, A., Dehn, A., Deters, B., Himmelmann, S., Voigt, S. and Orphal J.: Atmospheric remote-sensing reference data from GOME 2. Temperature-dependent absorption cross-sections of $O_3$ in the 231-794 nm range. J. Quant. Spectrosc. Radiat. Transfer, 61, 509–517, doi:10.1016/S0022-4073(98)00037-5, 1999.

Callies, J., Corpaccioli, E., Eisinger, M., Hahne, A., and Lefebvre, A.: GOME-2 – Metop?s second generation sensor for operational ozone monitoring, ESA Bull.-Eur. Space, 102, 28–36, 2000.

Caron, L., -P., Jones, C., G., Vaillancourt, P., A., and Winger, K.,: On the relationship between cloud-radiation interaction, atmospheric stability and Atlantic tropical cyclones in a variable-resolution climate model, Clim. Dyn., 40, 5–6, 1257–1269, doi:10.1007/s00382-012-1311-6, 2013.

Chance, K. V., and Spurr, R. J. D.: Ring effect studies: Rayleigh scattering, including molecular parameters for rotational Raman scattering, and the Fraunhofer spectrum, Appl. Opt., 36, 5224–5230, doi:10.1364/AO.36.005224, 1997.

Chance, K, and Kurucz, R.L.: An improved high-resolution solar reference spectrum for Earth's atmosphere measurements in the ultraviolet, visible, and near infrared, J. Quant. Spectrosc. Radiat. Transfer, 111, 1289–1295, doi:10.1016/j.jqsrt.2010.01.036, 2010.

Chadyšien, R., and Girgždys, A.: Ultraviolet Radiation Albedo of Natural Surfaces, J. Environ. Eng. Landsc., 16, 83–88, doi:10.3846/1648-6897.2008.16.83-88, 2008.

Charron, M., and co-authors: The stratospheric extension of the Canadian Global Deterministic Medium-Range Weather Forecasting System and its impact on tropospheric forecasts. Mon. Wea. Rev., 140, 1924–1944, doi:10.1175/MWR-D-11-00097.1, 2012.

CIE (International Commission on Illumination) Technical Report: Rationalizing nomenclature for UV doses and effects on humans. Joint publication of CIE and WMO (World Meteorological Organization), CIE 209:2014 - WMO/GAW Report No. 211, ISBN: 978-3-902842-35-0, 2014.

Colblentz, M. W., and Stair, R.: Data on the spectral erythemic reaction of the untanned human skin to ultraviolet radiation, Research Paper RP631, National Bureau of Standards Journal of Research 13, January (1934).

Crutzen, P. J.: Ultraviolet on the increase, Nature, 356, 104–105, doi:10.1038/356104a0, 1992.

de Grandpré, J., Tanguay, M., Qaddouri, A., Zerroukat, M., and McLinden, C. A.: Semi-Lagrangian Advection of Stratospheric Ozone on a Yin-Yang Grid System, Monthly Weather Review, 144, 1035–1050, doi:10.1175/MWR-D-15-0142.1, 2016.

Dobber, M., Voors, R., Dirksen, R., Kleipool, Q., and Levelt, P.: The High-Resolution Solar Reference Spectrum between 250 and 550 nm and its Application to Measurements with the Ozone Monitoring Instrument, Solar Phys., 249, 281–291, doi:10.1007/s11207-008-9187-7, 2008.

Fisher, M., and Andersson, E.: Developments in 4-D-Var and Kalman filtering, in: Technical Memorandum Research Department, 347, ECMWF, Reading, UK, 2001.

Fioletov, V. E., Kerr, J. B., and Wardle, D. I.: The relationship between total ozone and spectral UV irradiance from Brewer observations and its use for derivation of total ozone from UV measurements, Geophys. Res. Lett., 24, 2997–3000, doi:10.1029/97GL53153, 1997.

Fioletov, V., Kerr, J. B., and Fergusson, A.: The UV Index: Definition, Distribution and Factors Affecting It, Can. J. Public Health, 101(4), I5–I9, 2010.

Girard, C., Plante, A., Desgagné, M., McTaggart-Cowan, R., Côté, J., Charron, M., Gravel, S., Lee, V., Patoine, A., Qaddouri, A., Roch, M., Spacek, L., Tanguay, M., Vaillancourt, P. A., and Zadra, A.: Staggered Vertical Discretization of the Canadian Environmental Multiscale (GEM) Model Using a Coordinate of the Log-Hydrostatic-Pressure Type, Mon. Wea. Rev., 142, 1183–1196, doi:10.1175/MWR-D-13-00255.1, 2014.

Gong, W., Makar, P. A., Zhang, J., Milbrandt, J., Gravel, S., Hayden, K. L., Macdonald, A. M., and Leaith, W. R.: Modelling aerosol-cloud-meteorology interaction: a case study with a fully coupled air quality model (GEM-MACH), Atmos. Environ., 115, 695–715, doi:10.1016/j.atmosenv.2015.05.062, 2015.

Hall, L. A. and Anderson, G. P.: High resolution solar spectrum between 2000 and 3100 Angstroms, J. Geophys. Res., 96, 12927?12931, doi:10.1029/91JD01111, 1991.

He, H., Fioletov, V. E., Tarasick, D. W., Mathews, T. W., and Long, C.: Validation of Environment Canada and NOAA UV Index Forecasts with Brewer Measurements from Canada, J. Appl. Meteor. Climatol., 52, 1477–1489, doi:10.1175/JAMC-D-12-0286.1, 2013.

Jacquinet-Husson, N., Scott, N. A., Chédin, A., Crépeau, L., Armante, R., Capelle, V., Orphal, J., Coustenis, A., Boonne, C., Poulet-Crovisier, N., Barbe, A., Birk, M., Brown, L. R., Camy-Peyret, C., Claveau, C., Chance, K., Christidis, N., Clerbaux, C., Coheur, P. F., Dana, V., Daumont, L., De Backer-Barilly, M. R., Di Lonardo, G., Flaud, J. M., Goldman, A., Hamdouni, A., Hess, M., Hurley, M. D., Jacquemart, D., Kleiner, I., Köpke, P., Mandin, J. Y., Massie, S., Mikhailenko, S., Nemtchinov, V., Nikitin, A., Newnham, D., Perrin, A., Perevalov, V. I., Pinnock, S., Régalia-Jarlot, L., Rinsland, C. P., Rublev, A., Schreier, F., Schult, L., Smith, K. M., Tashkun, S. A., Teffo, J. L., Toth, R. A., Tyuterev, Vl. G., Auwera, J. V., Varanasi, P., and Wagner, G.: The GEISA spectroscopic database: Current and future archive for Earth and planetary atmosphere studies, J. Quant. Spectrosc. Radiat. Transfer, 109, 1043–1059, doi:10.1016/j.jqsrt.2007.12.015, 2008.

Kerr, J.B,: The Brewer Spectrometer, chapter 6 in UV Radiation in Global Climate Change: Measurements, Modeling and Effects on Ecosystems, e.d. W. Gao, D.L. Schmoldt, and J.R. Slusser, Tsinghua University Press, Beijing, and Springer-Verlag Berlin Heidelberg, 160–191, 2010.

Kleipool, Q. L., Dobber, M. R., de Haan, J. F., and Levelt, P. F.: Earth surface reflectance climatology from 3 years of OMI data, J. Geophys. Res., 113, doi:10.1029/2008JD010290, 2008.

Kurucz, R. L., Furenlid, I., Brault, J., Testerman, L.: Solar Flux Atlas from 296 to 1300 nm, National Solar Observatory, Sunspot, New Mexico, 1984. [Available for download at:http://kurucz.harvard.edu/sun/fluxatlas/]

Li, J., and Barker, H. W.: A radiation algorithm with correlation-*k* distribution. Part I: local thermal equilibrium, J. Atmos. Sci., 62, 286–309, doi:10.1175/JAS-3396.1, 2005.

Long, C. S., 2003: UV index forecasting practices around the world. WCRP/Stratospheric Processes And their Role in Climate (SPARC) Newsletter 21. [Available for download at: http://www.atmosp.physics.utoronto.ca/SPARC/News21/21_Long.html]

Marchenko, S. V., DeLand, M. T., and Lean, J. L.: Solar spectral irradiance variability in cycle 24: observations and models, J. Space Weather Space Clim., 6, A40, 1–12, doi:10.1051/swsc/2016036, 2016.

Markovic, M., Jones, C., Vaillancourt, P., A., Paquin, D., Winger, K., and Paquin-Ricard, D.: An Evaluation of the Surface Radiation Budget Over North America for a Suite of Regional Climate Models against Surface Station Observation, Clim. Dyn., 31, 7, 779–794, doi:10.1007/s00382-008-0378-6, 2008.

Mathes, K., and co-authors: Solar forcing for CMIP6 (v3.2), Geosci. Model Dev., 10, 2247–2302, doi:10.5194/gmd-10-2247-2017, 2017.

Matsumi, Y., Comes, F. J., Hancock, G., Hofzumahaus, A., Hynes, A. J. , Kawasaki, M., and Ravishankara, A. R.: Quantum yields for production of O(1D) in the ultraviolet photolysis of ozone: Recommendation based on evaluation of laboratory data, J. Geo. Res., 107, D3, ACH 1-1–ACH 1-12, doi:10.1029/2001JD000510, 2002.

McKinlay, A. F., and Diffey, B. L.: A reference action spectrum for ultraviolet induced erythema in human skin, CIE Research Note, 6(1), 17–22, 1987.

McLinden, C. A., Olson, S. C., Hannegan, B., Wild, O., Prather, M. J., and Sundet, J.: Stratospheric ozone in 3-D models: a simplified chemistry and the cross-tropopause flux, J. Geophys. Res., 105, 14653–14665, doi:10.1029/2000JD900124, 2000.

Moran, M. D., Menard, S., Talbot, D., Huang, P., Makar, P. A., Gong, W., Landry, H., Gravel, S., Gong, S., Crevier, L.-P., Kallaur, and A., Sassi, M.: Particulate-matter forecasting with GEM-MACH15, a new Canadian operational air quality forecast model. In: Steyn, D. G. Rao, S.T. (Eds.), Air Pollution Modelling and its Application XX. Springer, Dordrecht, 289–293, 2010.

Moshammer, P., Simic, S., and Haluza, D.: UV "Indices" - What Do They Indicate?, Int. J. Environ. Res. Public Health, 13, 1041, doi:10.3390/ijerph13101041, 2016.

Munro, R., Eisinger, M., Anderson, C., Callies, J., Corpaccioli, E., Lang, R., Lefebvre, A., Livschitz, Y., and Albinana, A.P.: GOME-2 on MetOp, Proc. of The 2006 EUMETSAT Meteorological Satellite Conference, Helsinki, Finland, 2006.

Paquin-Ricard, D., Jones, C., and Vaillancourt, P. A., : Using ARM Observations to Evaluate Cloud and Clear-Sky Radiation Processes as Simulated by the Canadian Regional Climate Model GEM, Mon. Wea. Rev., 138, 3, 818–838, doi:10.1175/2009MWR2745.1, 2010.

Prather, M. J.: Photolysis rates in correlated overlapping cloud fields: Cloud-J 7.3c Geosci. Model Dev., 8, 2587–2595, doi:10.5194/gmd-8-2587-2015, 2015.

Ravanat, J-, L., Douki, T., and Cadet, J.: Direct and indirect effects of UV radiation on DNA and its components, J. Photochem. Photobiol. B, 63, 88–102, doi:10.1016/S1011-1344(01)00206-8, 2001.

Rowland, F. S.: Stratospheric Ozone Depletion by Chlorofluorocarbons (Nobel Lecture) Angew Chem Int. Ed. Engl., 35, 1786–1798, doi:10.1002/anie.199617861, 1996.

Schmalwieser, A. W., Gröbner, J., Blumthaler, M., Klotz, B., De Backer, H., Bolsée, D., Werner, R., Tomsic, D., Metelka, L., Eriksen, P., Jepsen, N., Aun, M., Heikkilä, A., Duprat, T., Sandmann, H., Weiss, T., Bais, A., Toth, Z., Siani, A., Vaccaro, L., Diémoz, H., Grifoni, D., Zipoli, G., Lorenzetto, G., Petkov, B. H., di Sarra, A.G., Massen, F., Yousif, C., Aculinin, A. A., den Outer, P., Svendby, T., Dahlback, A., Johnsen, B., Biszczuk-Jakubowska, J., Krzyscin, J., Henriques, D., Chubarova, N., Kolarž, P., Mijatovic, Z., Groselj, D., Pribullova, A., Gonzales, J. R. M., Bilbao, J., Guerrero, J. M. V., Serrano, A., Andersson, S., Vuilleumier, L., Webb, A., and O'Hagan, J.:UV Index monitoring in Europe. Photochem. Photobiol. Sci.,16, 1349–1370, doi:10.1039/C7PP00178A, 2017.

Scinocca, J. F., McFarlane, A., Lazare, M., Li, J., and Plummer, D.: Technical Note: The CCCma third generation AGCM and its extension into the middle atmosphere, Atmos. Chem. Phys., 8, 7055–7074, doi:10.5194/acp-8-7055-2008.

Smith, G. C., Roy, F., Mann, P., Dupont, F., Brasnett, B., Lemieux, J. -F., Laroche, S., and Bélair, S.: A new atmospheric dataset for forcing ~~ice?ocean~~ ice-ocean models: Evaluation of reforecasts using the Canadian global deterministic prediction system, Q.J.R. Meteorol. Soc., 140, 881–894, doi:10.1002/qj.2194, 2014.

Sundqvist, H., Berge, E., Kristjansson, J. E.: Condensation and cloud parameterisation studies with a mesoscale numerical weather prediction model, Mon. Weather Rev., 117, 1641–1657, doi:10.1175/1520-0493(1989)117<1641:CACPSW>2.0.CO;2, 1989.

Thompson A., Early, E.A., DeLuisi, J., Disterhoft, P., Wardle, D., Kerr, J., Rives, J., Sun, Y., Lucas, T., Mestechkina, T., and Neale, P.: The 1994 North American interagency intercomparison of ultraviolet monitoring spectroradiometers. J. Res. Natl. Inst. Stand. Technol. 102, 279–322, 1997.

Thuillier, G., Hersé, M., Simon, P., Labs, D., Mandel, H., Gillotay, D., Foujols, T.: The Visible Solar Spectral Irradiance from 350 to 850 nm As Measured by the SOLSPEC Spectrometer During the ATLAS I Mission, Solar Phys. 177, 41-61, doi:10.1023/A:1004953215589, 1998.

Thuillier, G., Hersé, M., Labs, D., Foujols, T., Peetermans, W., Gillotay, D., Simon, P., Mandel, H.: The Solar Spectral Irradiance from 200 to 2400 nm as Measured by the SOLSPEC Spectrometer from the Atlas and Eureca Missions, Solar Phys. 214, 1-22, doi:10.1023/A:1024048429145, 2003.

Toon, O. B., and J. B. Pollack: A global average model of atmospheric aerosols for radiative transfer calculations, J. Appl. Meteor., 15, 225–246, doi:10.1175/1520-0450(1976)015<0225:AGAMOA>2.0.CO;2, 1976.

van der A, R.J., Allaart, M.A.F., and Eskes, H.J.: Extended and refined multi sensor reanalysis of total column for the period 1970-2012, Atmos. Meas. Tech., 8, 3021–3035, doi:10.5194/amt-8-3021-2015, 2015.

Voigt, S., Orphal, J., Bogumil, K., and Burrows, J. P.: The temperature dependence (203-293 K) of the absorption cross-sections of $O_3$ in the 230-850 nm region measured by Fourier-transform spectroscopy, J. Photochem. Photobiol., A , 143, 1–9, doi:10.1016/S1010-6030(01)00480-4, 2001.

von Salzen, K., Scinocca, J. F., McFarlane, N. A., Li, J., Cole, J. N. S., Plummer, D., Verseghy, D. , Reader, M. C., Ma, X., Lazare, M., and Solheim, L.: The Canadian Fourth Generation Atmospheric Global Climate Model (CanAM4). Part I: Representation of Physical Processes, Atmosphere-Ocean, 51, 104–125, doi:10.1080/07055900.2012.755610, 2013.

Webb, A. R., Slaper, H., Koepke, P., and Schmalwieser, A. W.: Know Your Standard: Clarifying the CIE Erythema Action Spectrum, Photochem. Photobiol., 87, 483–486, doi:10.1111/j.1751-1097.2010.00871.x, 2011.

Global Solar UV Index: A Practical Guide. A joint recommendation of the World Health Organization, World Meteorological Organization, United Nations Environment Programme, and the International Commission on Non-Ionizing Radiation Protection, ISBN: 92-4-159007-6 , 2002.

Wild, O., Zhu, X., and Prather, M. J.: Fast-J: Accurate simulation of in- and below-cloud photolysis in tropospheric chemical models, J. Atmos. Chem., 37, 245–282, doi:10.1023/A:1006415919030, 2000.

Yeo, K. L., Ball, W. T., Krivova, N. A., Solanki, S. K., Unruh, Y. C., and Morrill, J.: UV solar irradiance in observations and the NRLSSI and SATIRE-S models, J. Geophys. Res., 120, 6055–6070, doi:10.1002/2015JA021277, 2015.

Zadra, A., McTaggart-Cowan, R., Vaillancourt, P.A., Roch, M., Bélair, S., and Leduc, A.-M.: Evaluation of tropical cyclones in the Canadian Global Modeling System: Sensitivity to moist process parameterization. Mon. Wea. Rev., 142, 1197–1220, doi:10.1175/MWR-D-13-00124.1, 2014a.

Zadra, A, and co-authors: Improvements to the Global Deterministic Prediction system (GDPS) (from version 2.2.2 to 3.0.0), and related changes to the Regional Deterministic Prediction System (RDPS) (from version 3.0.0 to 3.1.0). Canadian Meteorological Centre Tech. Note, 88 pp., 2014b. [Available for download at: http://collaboration.cmc.ec.gc.ca/cmc/CMOI/product_guide/docs/lib/op_systems/doc_opchanges/technote_gdps300_20130213_e.pdf]

Zepp, R, G., Callaghan, T. V., and Erickson, D. J.: Effects of enhanced solar ultraviolet radiation on biogeochemical cycles, J. Photochem. Photobiol. B, 46, 69–82, doi:10.1016/S1011-1344(98)00186-90, 1998.